IR spectroscopy of Lipid/Lipid and Lipid/Protein interaction in bulk phases and monolayers

by Xin Xiao

A thesis submitted to the

Graduate School-Newark

Rutgers, The State University of New Jersey

in partial fulfillment of the requirements

for the degree of Master of Science

Graduate Program in Chemistry

written under the direction of

Richard Mendelsohn

and approved by

_____

_____

_____

_____

Newark, New Jersey

Oct. 2013

Abstract

The thesis consists of three parts. In the first part, the interaction between oleic acid and components of model stratum corneum (SC) lipids was investigated with Langmuir monolayer and associated techniques. The domain structure and lipid conformational order of the monolayers were studied through Infrared Reflectance Absorbance Spectrometry (IRRAS). Oleic acid was found to first mix and disorder the ceramide enriched domains and it only started to affect the palmtic acid enriched domain and disrupt the domain speartion in SC lipids at higher oleic acid percentage. In the second part, the effects of pH and temperature on components of model stratum corneum lipids were investigated with FTIR. At pH 5 and 7 components of model stratum corneum form an orthorhombic lattice under low temperatures whereas at pH 10 components form a hexagonal lattice. In the last part, the interactions between lung surfactant SP-D and PI were investigated with IRRAS. SP-D showed high PI or low PC affinity with the species-dependent preference for inositol.

Acknowledgements

I would like to gratefully acknowledge the enthusiastic supervision of Dr. Richard Mendelsohn.

Additionally, I thank Dr. Carol Flach for data analysis and relevant discussions.

I am grateful to all members of Dr. Mendelsohn's research group for their technical help and advice.

I am indebted to my family for their understanding, endless patience and encouragement.

Table of Contents

Part I Effects of Oleic Acid on the Structural Organization of Stratum Corneum Models

1.1 Introduction

Skin, the largest organ of the body and the outer covering of humans, performs the following functions: First, it serves as the barrier protecting the organism from pathogens and damage caused by the external environment [1]. Second, a variety of nerve endings in the skin respond to temperature, touch, pressure, etc. Third, skin plays an important role in controlling evaporation by providing a dry and semi-impermeable barrier to fluid loss [2]. Finally, skin is a storage medium for water and lipids. Minor functions of skin include facilitation of absorption of small amounts of oxygen, nitrogen and carbon dioxide into the epidermis.

Skin consists of two major layers. The epidermis provides the barriers to infection and water retention that are critical for maintaining healthy skin. The dermis provides energy and nutrients to the epidermis and plays an important role in themoregulation and in healing.

The stratum corneum, Figure 1.1, is the outmost boundary of the epidermis and is composed of 4 or 5 layers [3]. Those layers [4] in descending order into the skin are the cornified layer (stratum corneum or SC), the clear layer (stratum lucidum), the granular layer (stratum granulosum), the spinous layer (stratum spinosum) and the basal layer (stratum basale). The chemical and biological activities of the SC are very complex. A “brick and mortar” type structure has been described for its structure.

Stratum corneum consists of 12—16 layers of cornecytes (dead cells) filled with the water-retaining protein keratin surrounded in the extracellular space by stacked layers of lipids. These cornecytes are considered to be the bricks composed of keratin in an organized matrix. Keratin retains large amounts of water. Specific protein structures called corneodesmosomes can link cornecytes together. These proteins are one part of the mortar in the standard "brick and mortar" model. The lipids filling the spaces are the other part of the mortar. The lipids play a major role in maintaining the barrier properties of skin. In a widely used lipid model for human stratum corneum [5], the lipid composition is an eqimolar mixture of ceramides(CERs), free fatty acids(FFAs), and cholesterol(CHOL). Other lipids which are present include cholesterol sulphate, glucosylceramides and cholesterol esters.

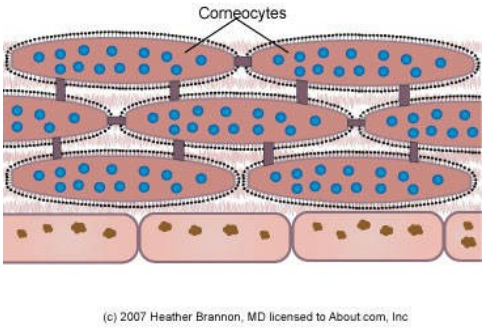

Figure 1.1 The structure of stratum corneum

Ceramides are responsible for the barrier-forming and moisture-binding functions of the complex lipid mixture in the SC. At least eleven ceramide structures [6] are present in human SC Figure 1.3. The head groups of ceramides with several

functional groups can form hydrogen bonds with adjacent molecules. Ceramides have been classified into four types: sphingosine, phytosphingosine, 6-hydroxysphingosine and dihydrosphingosine, all of which describe the nature of their base chains. There are three variations in structure of the fatty acids linked to the base, namely non-hydroxylated fatty acid (N), α-hydroxy fatty acid (A), or ω-hydroxy fatty acid. Four bases with fatty acids result in eight ceramide structures, referred to as AS, AP, AH, AD and NS, NP, NH and ND. Furthermore, linoleic acid is linked to the ω-hydroxy group, which results in 3 additional ceramides, referred to as EOS, EOH and EOP.

The structure of free fatty acids in the SC is predominately long-chain (C20-C30) and saturated. The biological behavior of cholesterol in stratum corneum is very complicated. Cholesterol can decrease the chain mobility and therefore tends to destabilize lipids in the liquid phase [7]. But cholesterol also can increase chain mobility and reduce chain packing in ordered gel phases [8].

Lipid organization, Figure1.2, is very important for skin barrier function. Lateral packing and the nature of the lamellar phases were found to be important for human SC. Two lamellar phases [8] are present in human SC: one lamellar phase has a periodicity of ~ 6 nm and is called the SPP (short periodicity phase) while the other lamellar phase has a periodicity of ~ 13 nm and is called the LLP (long periodicity phase). The LLP is present in almost all species, and therefore LLP is suggested as playing an important role in skin barrier functions. In the plane perpendicular to the direction of lamellar phases, the lipids are arranged in one of three forms, a liquid phase, a hexagonal phase or a phase with orthorhombic lateral packing. The phases that have

orthorhombic geometries are very densely packed. Some studies [10][11] have shown the orthorhombic lateral packing is present in the human stratum corneum. Recently it has been proven that there is a correlation between orthorhombic lateral packing and trans-epidermal water loss [12], a measure of skin barrier function. The conclusion is that orthorhombic lateral packing plays an important role in skin barrier function.

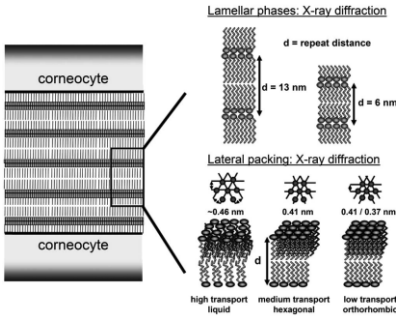

Figure 1.2 A schematic drawing of the lamellar in the human stratum corneum. [Joke A. Bouwstra and Gert S. Gooris *The Open Dermatology Journal,(2010), Vol. 4, 10-13*]

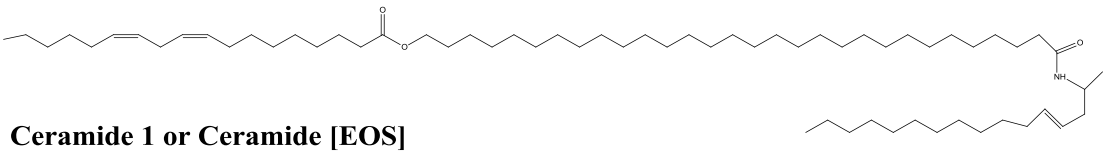

Ceramide 1 or Ceramide [EOS]

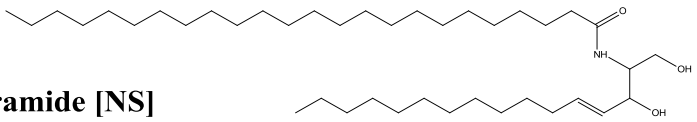

Ceramide 2 or Ceramide [NS]

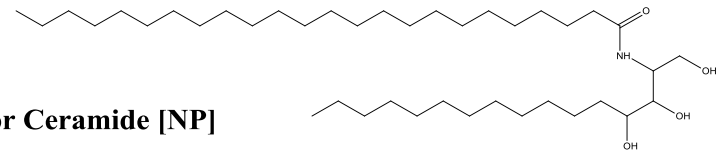

Ceramide 3 or Ceramide [NP]

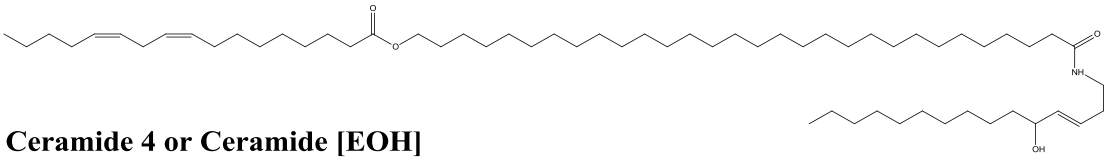

Ceramide 4 or Ceramide [EOH]

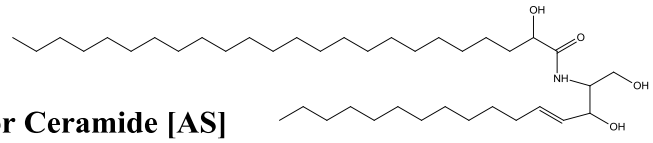

Ceramide 5 or Ceramide [AS]

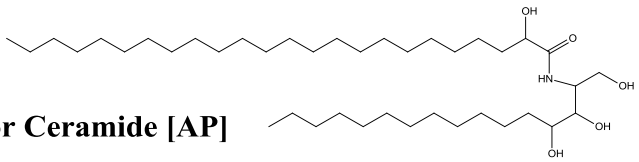

Ceramide 6 or Ceramide [AP]

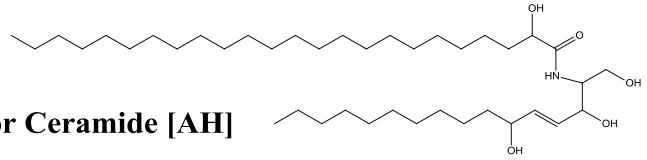

Ceramide 7 or Ceramide [AH]

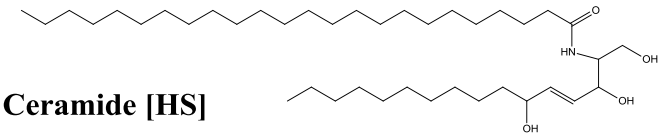

Ceramide 8 or Ceramide [HS]

Figure 1.3 The chemical structure of human stratum corneum ceramides. [Robson et al., (1994) *J. Lipid Res*. 35: 2060-2068; Stewart et. al., (1999) *J. Lipid Res.* 1999, 40: 1434-1439]

An interesting point arises as skin is a very good barrier to foreign substances. But sometimes it is required that materials penetrate into the skin. So the concept of skin penetration enhancers was put forward. What are "skin penetration enhancers"? A skin penetration enhancer can decrease the barrier resistance of the stratum corneum and allow drugs and lubricants to be absorbed into skin and eventually into the systemic circulation [13]. In other words, skin penetration enhancers can alter the physical and chemical properties of the stratum corneum to allow substances to penetrate into the lower layers of skin. Some skincare and cosmetic products contain skin penetration enhancers. For example, to increase moisturization, humectants that are substances primarily used in foods and cosmetic products to promote retention of moisture, need to permeate into the skin. Skin penetration enhancers work by interacting with the lipids in the stratum corneum. They may interact at the polar head groups of the lipids, within water regions between the head groups of the lipids, or between the lipophilic tails of the bilayer. Skin penetration enhancers also react with keratin fibrils and their associated water in the corneocyte. Partitioning processes may be changed due to the high concentration of solvent. Because of the involvement of lipids and protein in the partitioning process, lipid/protein partitioning theory (LPP) has been adapted to explain the mechanism of permeation enhancement. The theory has been utilized for data analysis applied to water, azone, oleic acid, propylene glycol, sodium lauryl sulphate,

dimethylformamide, 2-pyrrolidone, dimethylsulphoxide and decylmethylsulphoxide [13].

Oleic acid is a fatty acid present in various animals and vegetable fats and oils. It is a monounsaturated cis omega-9 fatty acid with a formula $CH_3(CH_2)_7CH=CH(CH_2)_7COOH$. Oleic acid is commonly used as an emollient and textile modifier in skincare products. As mentioned above, oleic acid is a well-known skin penetration enhancer which increases skin permeability. The mode of action of oleic acid has been previously investigated [14]. Two mechanistic scenarios of oleic acid as a skin penetration enhancer have been formulated: lipid fluidization and lipid phase separation. Francoeur et al[15] observed that deuterated oleic acid lowered the SC lipid phase transition temperature (T_m) in both isolated SC sheets and extracted SC lipid dispersions, but did not change SC lipid acyl chain order at temperatures below T_m. They suggested that oleic acid enhances skin permeation by forming a separate disordered oleic acid phase in SC lipids. However, Guy et al[16] reported that deuterated oleic acid increased SC lipid disorder in an in vivo ATR-IR study and showed that such disordering effects correlate with depth into the SC. In their study, oleic acid decreased the viscosity of the lipid only in the top layers of the stratum corneum. Additionally, while the intercellular lipids exist in the solid state, oleic acid is found to exist in its liquid phase. They therefore proposed that oleic acid enhances skin permeability through a duel mechanism involving disordering of the SC lipid and phase separation, with the latter effect predominating. In a 2H NMR study, Thewalt et al[17] found that

oleic acid did not alter the melting temperature of a model SC lipid, but did extract some SC lipids and promoted phase separation in SC lipids.

Infrared spectroscopy (IR) is a technique that measures the frequencies of molecular vibrations. The IR spectrum is usually divided into three regions: near-IR (0.8-2.5 um wavelength), mid-IR (2.5-25 um wavelength) and far-IR (25-1000 um wavelength) regimes. The mid-IR is often used to study fundamental vibrations and associated rotational-vibrational structure in the gas phase. The main use of this technique is to identify and analyze molecular structure. Fourier transform infrared spectroscopy (FTIR), a common laboratory technique, has become a very valuable tool to study biomolecules in biological and medical areas [18]. Several additional combined research techniques have been derived from FTIR, such as ATR-FTIR, GC-FTIR and HPLC-FTIR [19].

Biomolecules undergo vibrational transitions when absorbing infrared specific frequencies which match the transition energy of the bonds or atomic groupings that vibrate. The IR energies are determined by the shape of the molecular potential energy surfaces and the mass of the atoms. So the infrared spectrum can provide some useful information about changes in molecular conformation. When a vibrational mode is considered to be 'IR' active, it must be associated with a change in the dipole moment. A molecule vibrates in many ways, and each way is called a normal vibrational mode. Some fundamental vibrational modes from IR spectra related to the stratum corneum are discussed below.

Characteristic infrared acyl chain group vibrations, Figure 1.4, and head group vibrations, Figure 1.5, are used to analyze stratum corneum lipid organization. The CH_2 stretching (2800 cm-^{1}–3000 cm^{-1}) and CD_2 stretching (2000 cm^{-1}–2200 cm^{-1}) modes are associated with lipid chains. The positions of the symmetric and asymmetric stretching frequencies are sensitive mostly to the trans/gauche population ratio in the acyl chains. The lower frequency symmetric stretching mode is usually used to study conformations in lipid mixtures. The shift of these frequencies with temperature provides information about alterations in lipid conformation order [20] and phase transitions.

The CH_2 chain scissoring modes between 1462 cm^{-1} and 1474 cm^{-1} and its perdeuterated chain scissoring analogues between 1085 cm^{-1} and 1092 cm^{-1} are useful for the study of lateral hydrocarbon chain packing arrangements and domain sizes. Some studies [21][22] have shown that the magnitude of the splitting or broadening is an indication of domain size of

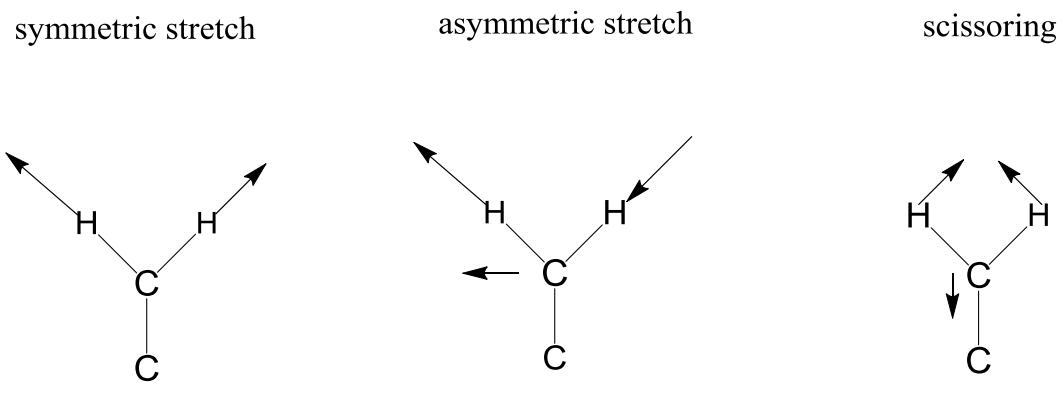

2846 - 2855 cm^{-1} 2915 - 2925 cm^{-1} 1462 - 1474 cm^{-1}

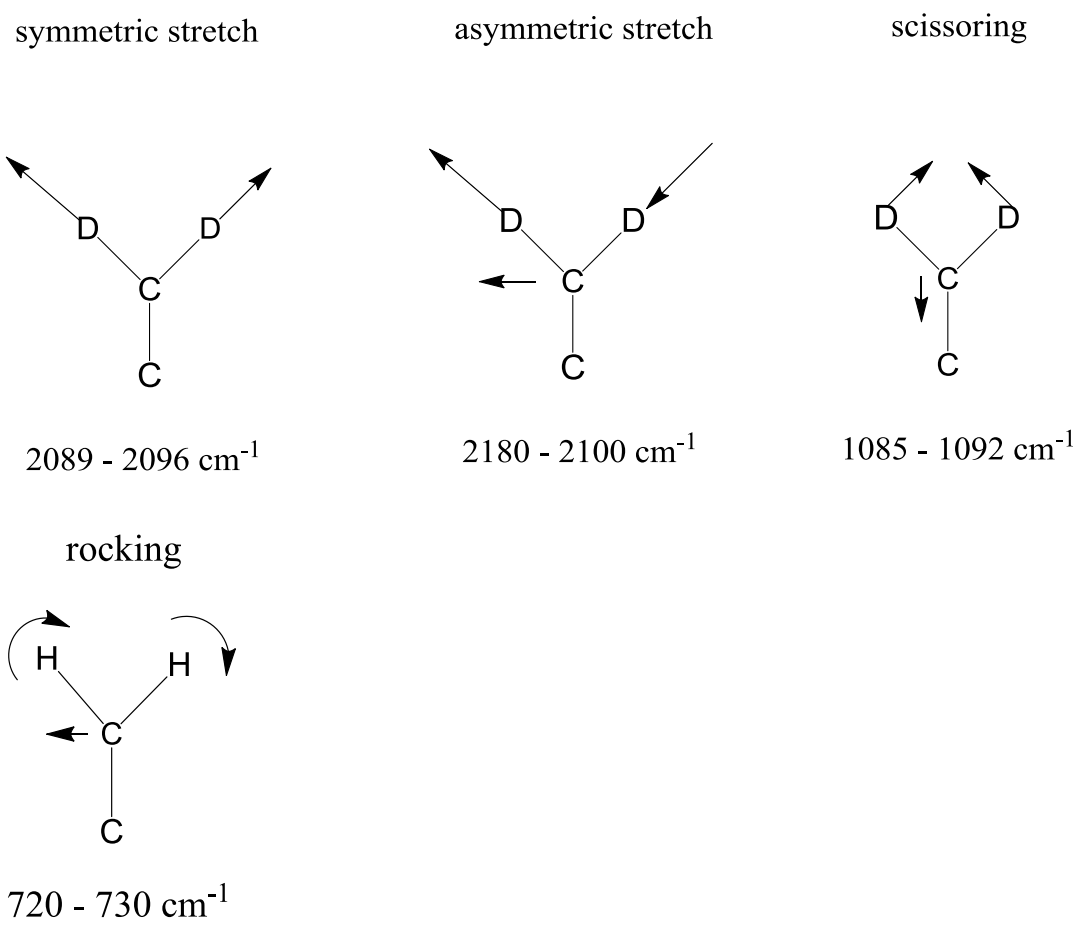

Figure 1.4 CH_2 and CD_2 stretching, scissoring and rocking modes are shown.

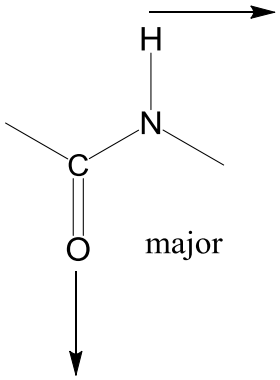

Amide I: 1615 - 1690 cm^{-1}

(a)

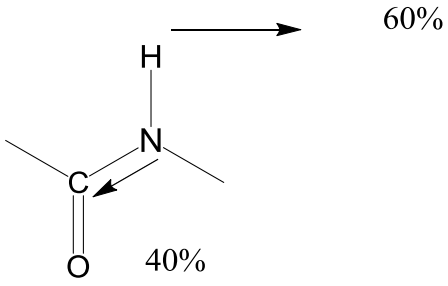

Amide II: 1520 - 1560 cm^{-1}

(b)

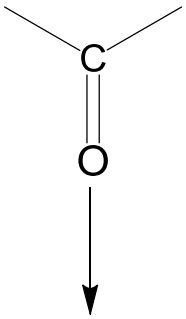

acid carbonyl: 1720 - 1750 cm^{-1}

(c)

Figure 1.5 The amide I (a) arises from 80% C=O stretch of the peptide bond. The amide II (b) arises from a normal mode consisting of 60% N-H in-plane bend and 40% C-N stretch. The acid C=O stretching mode (c) is used to probe the role of H-bonding in the study of lipid organization.

orthorhombic phases. The rocking vibration modes also are used to monitor the packing of the lipid acyl chains [23].

The Amide I and Amide II vibrational modes of amide groups [24] are important for protein secondary structure analysis. They are also useful to study the polar regions of straturm corneum lipid headgroups in which ceramides contain these two amide groups. The amide I mode is sensitive to hydrogen bonding and arises from C=O stretching. The amide II arises from a mixture of N-H in plane bending and C-N stretching. The water H-O-H bending mode at 1645 cm^{-1} is very strong, which interferes with the amide I band. Therefore, deuterium oxide (D_2O) is often used to replace water as solvent. The exchange of amide protons with D_2O is a very useful means to characterize solvent exposure in proteins. While the amide I mode is shifted to only slightly (5-10 cm^{-1}) lower frequency, the amide II is shifted from 1550 cm^{-1} to 1450 cm^{-1} due to H→D exchange. O-H/N-H stretching intensities can be also monitored to monitor H→D exchange as a function of temperature.

1.2 Experimental Methodology

Material

Bovine brain ceramide (type III), cholesterol, palmitic acid, palmitic acid-d_{31} (98 atom % D), oleic acid, and oleic acid-d_{34} (98 atom % D) were purchased from Sigma-Aldrich (St. Louis, MO) and were used without additional purification. The ceramide used in this study belongs to the NS ceramide family with nonhydroxy fatty acid chains composed of predominantly stearic acid (C18:0) and nervonic acids (C24:1) attached

to a sphingosine headgroup through an amide bond. The structures of the ceramide, cholesterol and fatty acid are shown in Figure 1.6.

All materials were used without further purification. Sodium chloride, EDTA, HPLC grade H_2O, methanol and chloroform were all purchased from Fisher Scientific (Hampton, NH).

Sample Preparation

Ceramide, cholesterol, palmitic acid-d_{31}, oleic acid, and oleic acid-d_{34} were dissolved separately in chloroform at approximately 1.00 mg/ml. Individual solutions were combined to make the appropriate solutions. In our experiments, the molar ratios of the mixtures of ceramide, cholesterol and palmitic acid-d_{31} (equal molar ratio) to oleic acid or oleic acid-d_{34} are 60%:40%, 70%:30% and 80%:20%. The solutions were kept at -20 °C and the collection of all the isotherms were completed within 3 weeks to minimize the effect of solvent evaporation and lipid oxidation. A Nima 611 LB trough (Nima Technology, Inc., Coventry, England; maximium surface area approximately 600 cm^2) with a model PS4 surface pressure sensor was used for the acquisition of surface pressure-molecular area (π-A) isotherms from the four component mixtures. Generally, in all experiments, 10ul of

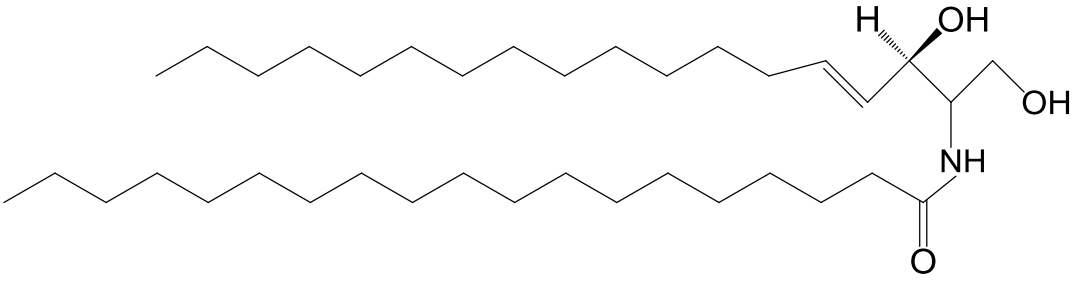

Bovine brain ceramide

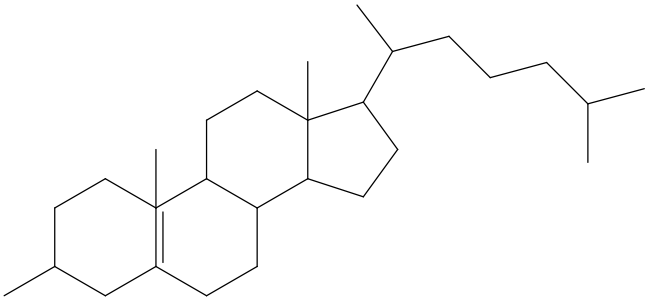

Cholesterol

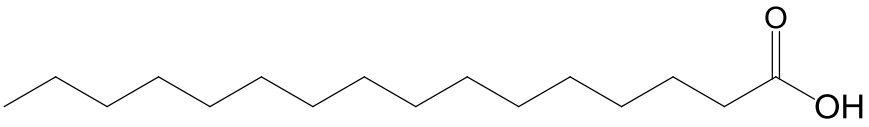

Palmitic acid

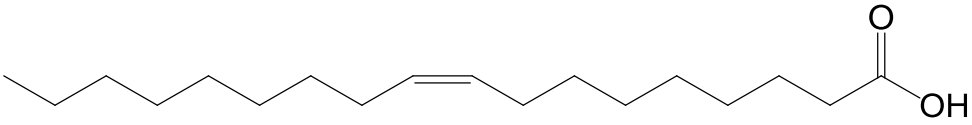

Oleic acid

Figure 1.6 Chemical structures of ceramide, cholesterol and fatty acids

the mixture of four components at different concentrations were spread on a 150 mM NaCl, 5 mM Tris buffer (pH=7.1), and 4 mM $CaCl_2$ subphase around 20°C at large molecular areas. Following a 15 min equilibration period to allow for solvent evaporation and film relaxation, monolayers were compressed at 15 cm^2/min while isotherms were recorded.

IRRAS measurements

Infrared reflection-absorption spectroscopy (IRRAS) provides molecular structure information from monolayer films at the air/water interface. IR spectra were acquired with a Bruker Instruments, Equinox 55 Spectrometer, equipped with an external variable angle reflectance accessory, the XA51. The IRRAS accessory is coupled to a custom-designed Langmuir trough with maximum surface area of 98 cm^2 constructed by Nima Technology (currently KSV NIMA). The IR beam was directed through a wire grid polarizer mounted in the optical path to the air/water interface with adjustable angle of incidence and collected with an HgCdTe detector. The entire accessory setup is enclosed and purged with nitrogen to maintain a stable low relative humidity to minimize water vapor interference. The trough can be shuttled to different positions relative to XA51 for interferograms collections at film-covered area as sample (with intensity R) and at uncovered area as background (with intensity R_0). Frequent updates of background interferograms helped to compensate the residual water vapor. IRRAS spectra are reported as $-\log(R/R_0)$ vs wavenumbers.

Lipid monolayers were compressed with one barrier moving from the end of the trough towards the surface pressure sensor at the other end at a speed of 2 cm^2/min. The barrier was stopped at surface pressures of interest and IRRAS spectra were collected at intermittent compressions while π-A isotherms were recorded. After 5 minutes of monolayer relaxation at each desired surface pressure, spectra were collected using s-polarized light at a 50° angle of incidence. For each spectrum, a total of 1024 scans were acquired at ~8 cm^{-1} resolution in 2 blocks of 512 scans each, co-added, apodized

with a Blackman-Harris-3-term function and fast Fourier transformed with one level of zero-filling to produce spectral data encoded at ~4 cm^{-1} intervals. All the experiments were duplicated, and the average results are reported here.

IRRAS data were analyzed with Grams/32 software (Galactic Industries Corp., Salem, NH) and peak positions of methylene stretching mode were determined with a center-of-gravity algorithm written by D. Moffatt and kindly provided by the National Research Council of Canada.

1.3 Results and Discussion

The methylene-stretching modes (νCH_2) between 2800-3000 cm^{-1} can be readily adopted to monitor lipid acyl chain order: a lower stretching frequency corresponds to more ordered acyl chains. Cholesterol has only a minor contribution to the methylene stretching band intensity, compared to the ceramide [25]. To monitor the ceramide and palmitic acid components in SC lipid monolayers separately, acyl chain perdeuterated palmitic acid was used in the IRRAS study. The use of deuterium isotope shifts the methylene stretching band to 2050-2250 cm^{-1} for νCD_2 and thus the ceramide and palmitic acid can be monitored separately from the same monolayer with IRRAS.

Typical νCH_2 and νCD_2 region of the IRRAS spectra from Cer/Chol/PA-d_{31} monolayers are shown in Figure 1.7a. Spectra are displayed at increasing surface pressures from top to bottom. The methylene asymmetric stretching ($\nu_{asym}CH_2$) frequencies arising from the ceramide component were determined based on a center of gravity algorithm and are presented as the black symbol in Figure 1.7b. The $\nu_{asym}CH_2$ frequencies from both the ceramide and palmitic acid components in the Cer/Chol/PA

monolayer are also shown for comparison as gray symbols. The $\nu_{asym}CH_2$ frequencies for both mixtures decreased with increasing surface pressure, especially for those lower than 10 mN/m. It is also obvious that the $\nu_{asym}CH_2$ frequencies for ceramide in Cer/Chol/PA-d_{31} is about 1.2 cm^{-1} higher than that for the sum of ceramide and palmitic acid in Cer/Chol/PA. This suggests that palmitic acid is more ordered than ceramide in SC lipid monolayer. It is thus reasonable to conclude that ceramide and palmitic acid did not exist in the same phase (on average)

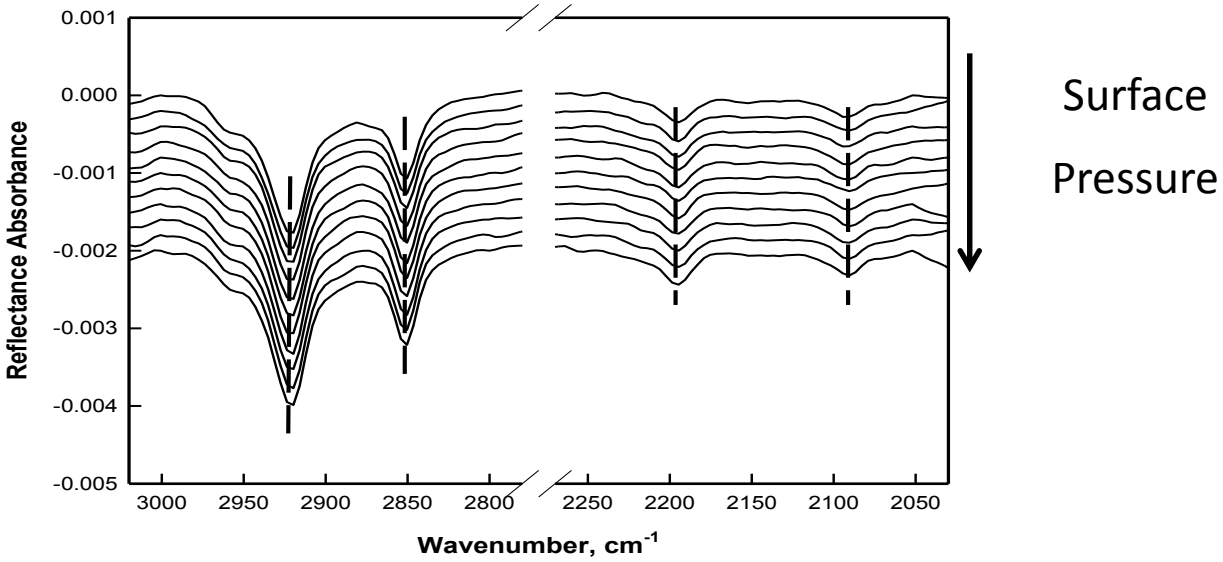

(a)

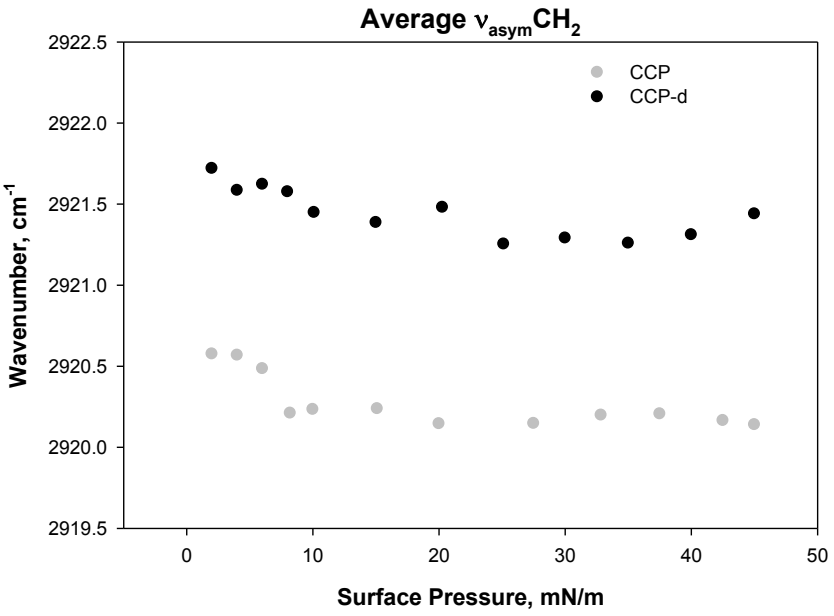

(b)

Figure 1.7 **a.** IRRAS spectra for Cer/Chol/PA-d at various surface pressure; b**.** Asymmetric CH_2 stretching frequency for Cer/Chol/PA-d (CCP-d) and Cer/Chol/PA (CCP).

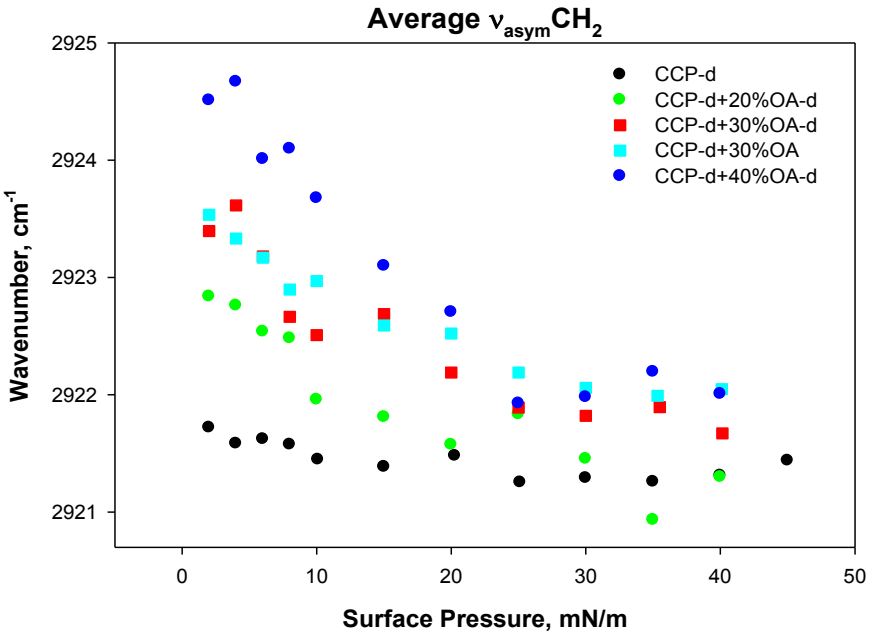

(a)

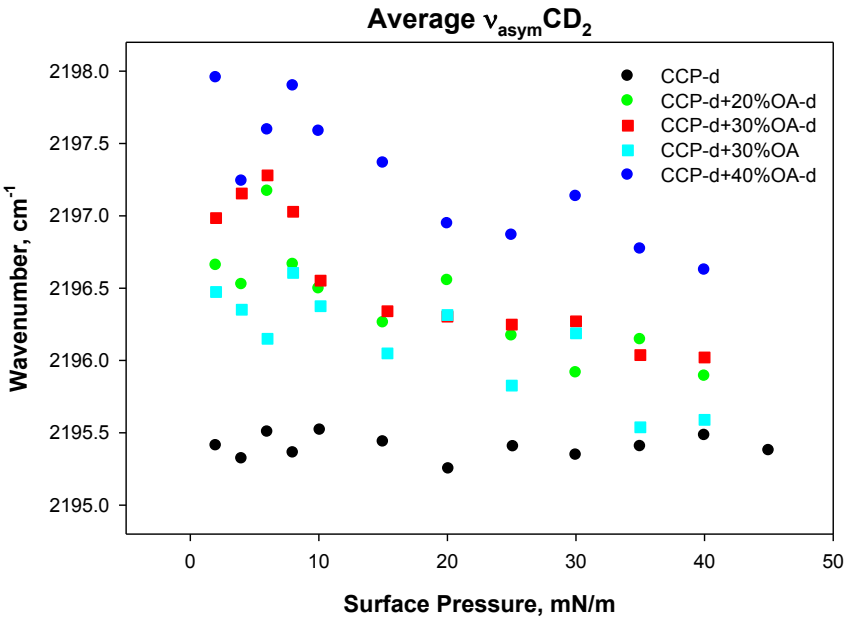

(b)

Figure 1.8 **a.** Asymmetric CH_2 stretching frequency for Cer/Chol/PA-d with 0 mol% , 20 mol% , 30 mol% and 40 mol% OA-d, and Cer/Chol/PA with 30% OA; **b.** Asymmetric CD_2 stretching frequency for Cer/Chol/PA-d with 0 mol% and 30 mol% OA-d and Cer/Chol/PA-d with 30 mol% OA

since they would tend to have the same conformational order if they were miscible in the same domain.

Deuterated OA (OA-d_{34}) was added to Cer/Chol/PA-d_{31} monolayers at 30% to evaluate its effect on ceramide acyl chain order. The $\nu_{asym}CH_2$ frequencies for ceramide at different surface pressures with and without 30%OA-d_{34} are shown in Figure 1.8a. OA-d_{34} increased $\nu_{asym}CH_2$ for ceramide over the full surface pressure range with increases up to 1.7 cm^{-1} at low surface pressures. OA-d_{34} clearly disordered the ceramide acyl chains. Similarly, 30% proteated oleic acid was added to Cer/Chol/PA-d_{31} to study the interaction between oleic acid and palmitic acid. The $\nu_{asym}CD_2$ frequencies of PA-d_{31} in Cer/Chol/PA-d_{31} monolayers with and without the presence of OA are shown in Figure 1.8b. The νCD_2 spectra from PA-d_{31} are noisier than the νCH_2 from ceramide due to the much smaller band intensity and thus the frequency data display more scatter. The νCD_2 frequencies were also 0.5-1 cm^{-1} higher in the presence of 30% OA at low surface pressure, but converged to the same value as that of Cer/Chol/PA-d_{31} at 35 mN/m and 40 mN/m. Palmitic acid was disordered by oleic acid at mostly low surface pressures and to a smaller extent at higher pressures since a smaller frequency increase was observed.

The interaction between oleic acid and ceramide or palmitic acid was further studied by comparing acyl chain stretching frequencies νCH_2 from both ceramide and oleic acid which are also plotted in Figure 1.8a, which overlaps the νCH_2 arising only from the ceramide component in Cer/Chol/PA- d_{31}+30% OA-d_{34}. The acyl chain order of ceramide and oleic acid in the mixture were similar, indicating they were likely to

exist in the same domain. The frequencies for νCD_2 from PA-d_{31} in Cer/Chol/PA-d_{31}+30% OA and those from PA-d_{31} and OA-d_{34} from Cer/Chol/PA-d_{31}+30% OA-d_{34} were compared in Figure 1.8b. The νCD_2 frequencies for PA-d_{31} and OA-d_{31} are ~0.5 cm^{-1} higher than those for PA-d_{31} at most surface pressures measured, indicating that oleic acid is more disordered than palmitic acid in the mixture. Thus they were not completely miscible in the monolayer and may be enriched in different domains.

Overall, the IRRAS results showed that oleic acid disordered both ceramide and palmitic acid but to a lesser extent for the latter. At 30% concentration in the mixture, oleic acid was observed to be completely miscible with ceramide and partially phase separated from palmitic acid. This is consistent with the previous discussion that oleic acid first interacted with the ceramide-enriched domain and then at higher concentrations interacted with the palmitic acid-enriched domain. The disordering effects observed in palmitic acid at 30% oleic acid could possibly arise from the interaction between oleic acid and palmitic acid mixed in the ceramide-enriched domain.

Part II Bulk Phase Organization of NFA Ceramide/Fatty Acid/Cholesterol: Effect of pH and Temperature

2.1 Introduction

Many biophysical studies [26] have demonstrated temperature-induced changes in the molecular organization of SC lipids. The thermotropic response and infrared spectra of equimolar CHOL/CER/FFA mixtures [26] shows that SC lipids exhibit a low-temperature transition near 35°C from an orthorhombic to a hexagonal phase and a transition from an ordered to a disordered phase at 60 to 80°C.

Stratum corneum pH plays an important role in skin barrier function [27]. Some skin diseases such as atopic dermatitis (AD), irritant contact dermatitis, and ichthyosis vulgaris express an elevated skin surface pH [28]. Increased pH values on the surface of lesional skin in AD patients compared with healthy skin have already been reported by Sparavigna et al [29]. Also, though skin barrier function physically is normal, newborn infants express an elevated skin surface pH for a couple of weeks postnatally. On the other hand, newborn infants have a high susceptibility for development of irritant contact dermatitis, indicating an impaired skin barrier function.

Three components of the SC lipids play important roles in the regulation of the rigidity of the lipid bilayer. For example, protonation of anionic forms of the fatty acids possibly affect the fluidity of the lipid bilayer. It is important to determine the effect of pH on the behavior of fatty acids in the lamellar lipids. X-ray diffraction studies of isolated ceramides, cholesterol and FFAs have reported a pH dependence on the

lamellar lipid organization [30]. In spite of these studies, little is known about the intermolecular interactions between the intercellar lamellar lipids. Fourier transform infrared spectroscopy (FTIR) can provide information about the nature of molecular interactions and information about the temperature and pH influences on lipid organization.

2.2 Experimental Methodology

Material

Porcine brain ceramide,(nonhydroxy fatty acid spingosine ceramide), was purchased from Avanti Polar Lipids, Inc. Cholesterol was obtained from Sigma-Aldrich, and perdeuterated stearic acid was purchased from Cambridge Isotope Laboratories, Inc. The structures of these three components are shown in Figure 2.1. Sodium chloride, EDTA, HPLC grade H_2O, methanol and chloroform were all purchased from Fisher Scientific (Hampton, NH). All the solvents and chemicals used were of analytical grade.

Sample preparations

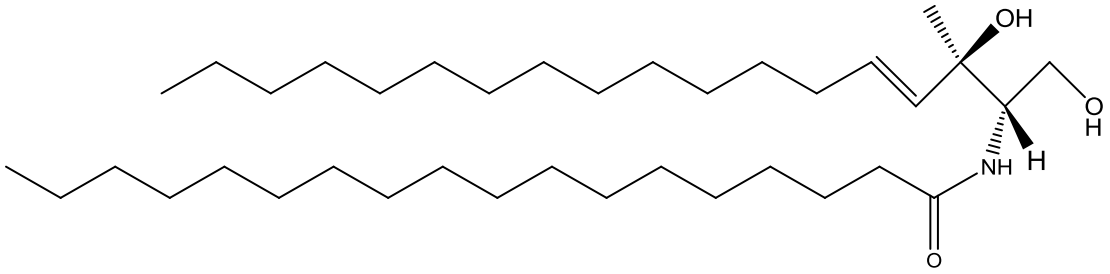

Porcine brain ceramide

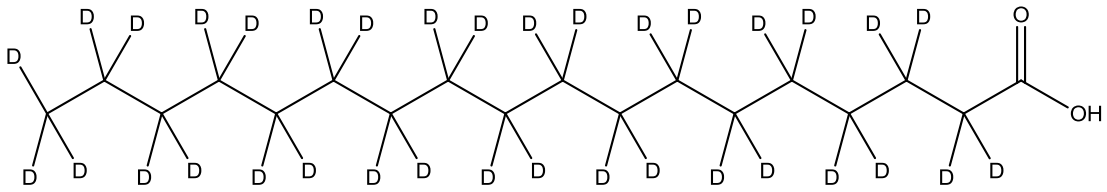

Stearic Acid-d_{35}

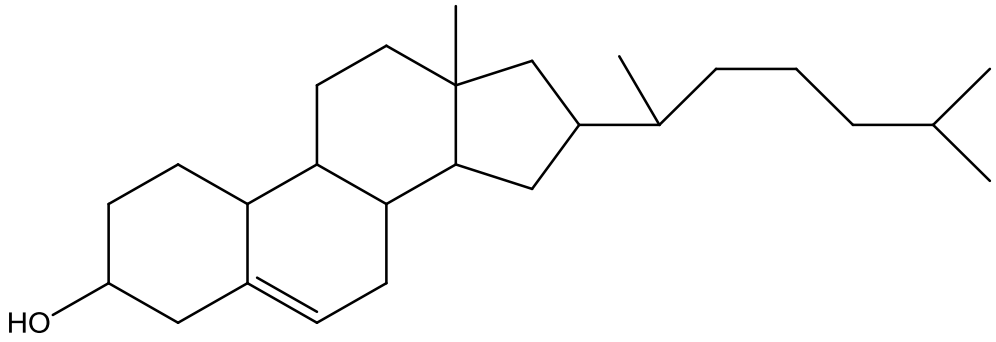

Cholesterol

Figure 2.1 The chemical structures of ceramide, fatty acid and cholesterol

Equimolar samples of ceramide, cholesterol and fatty acid were prepared by co-dissolving the lipids in a mixed chloroform/methanol (9:1)

solution, removing the solvent with dry N_2 and vacuum for at least 3 hours, after which the lipids were hydrated in 25 μL buffer. Six different buffers were prepared: pH 5.5 citrate buffer (H_2O, D_2O), pH 7 tris buffer (H_2O, D_2O) and pH10 sodium bicarbonate buffer (H_2O, D_2O). The lipids were heated at around 80°C and mixed by vortex action

repeatedly in order to ensure complete hydration and homogenization. The resultant dispersions were stored at 34.5°C overnight.

FTIR spectroscopy

All hydrated samples were heated to 80°C with periodical mixing. Following mixing, samples were sandwiched between ZnSe IR windows and mounted in a temperature-controlled transmission cell (Harrick Scientific, Ossining, NY). The starting temperature was set at 35°C for 1 hr and then reduced to 21°C. When the desired temperature was achieved, spectra were acquired routinely at 2°C or 5°C intervals from 21°C to 90°C.

Fourier transform infrared (FTIR) spectra were collected on a Mattson spectrometer equipped with a sample shuttle and a broad-band mercury- cadmium-telluride (MCT) detector. Spectra were generated from co-addition of 128 interferograms collected at 2 cm^{-1} resolution. Spectra were analyzed off-line using software written at the National Research Council of Canada and data were plotted with Sigma Plot 2000 (SCSS, Chicago).

2.3 Results and Discussion

The methylene stretching modes provide important information about the phase transition of skin lipids [31]. By using deuterated FFAs, the information on thermal behaviors of ceramide and FFAs can be obtained separately and simultaneously. The CH_2 (~2850 cm^{-1}) symmetric stretching bands and CD_2 (~2195 cm^{-1}) asymmetric

stretching bands have been used to investigate the thermotropism of ceramide and FFAs, respectively.

FTIR spectral analysis of the equimolar ratio of Cer/SA-d_{35}/Chol at pH 5.5, 7.0 and 10.0 have revealed that CER and SA-d_{35} in the mixture of three components exhibit complex thermotropic behaviors which vary with pH. The thermal behavior of CH_2 symmetric stretching band is shown in Figure 2.2. For the systems at pH 5.5 and pH 7.0, $\nu_s CH_2$ bands are located below 2850 cm^{-1} between 20°C and 40°C, which indicates that the acyl chains are highly ordered in this temperature range. As temperature increases, $\nu_s CH_2$ bands shift towards higher wavenumber, which is an indication of the disordering of the acyl chains. The thermal pattern at pH 5.5 and pH 7 in the CH_2 stretching region is characterized by a cooperative increase between 42°C and 62°C and between 44°C and 67°C

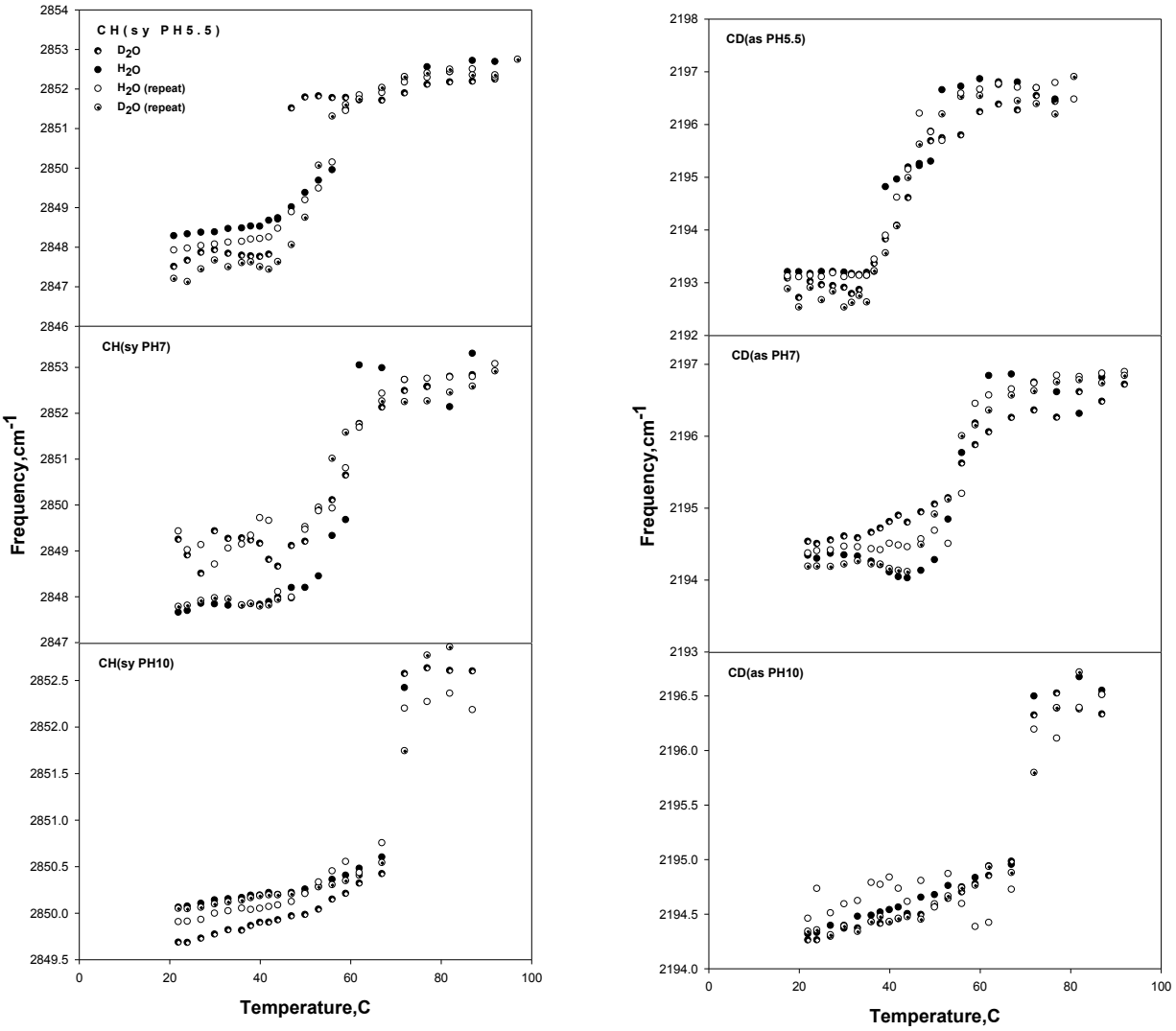

Figure 2.2 Thermotropism of equimolar mixtures of Cer/SA-d_{35}/Chol as probed with the ν_s CH_2 and ν_{as} CD_2

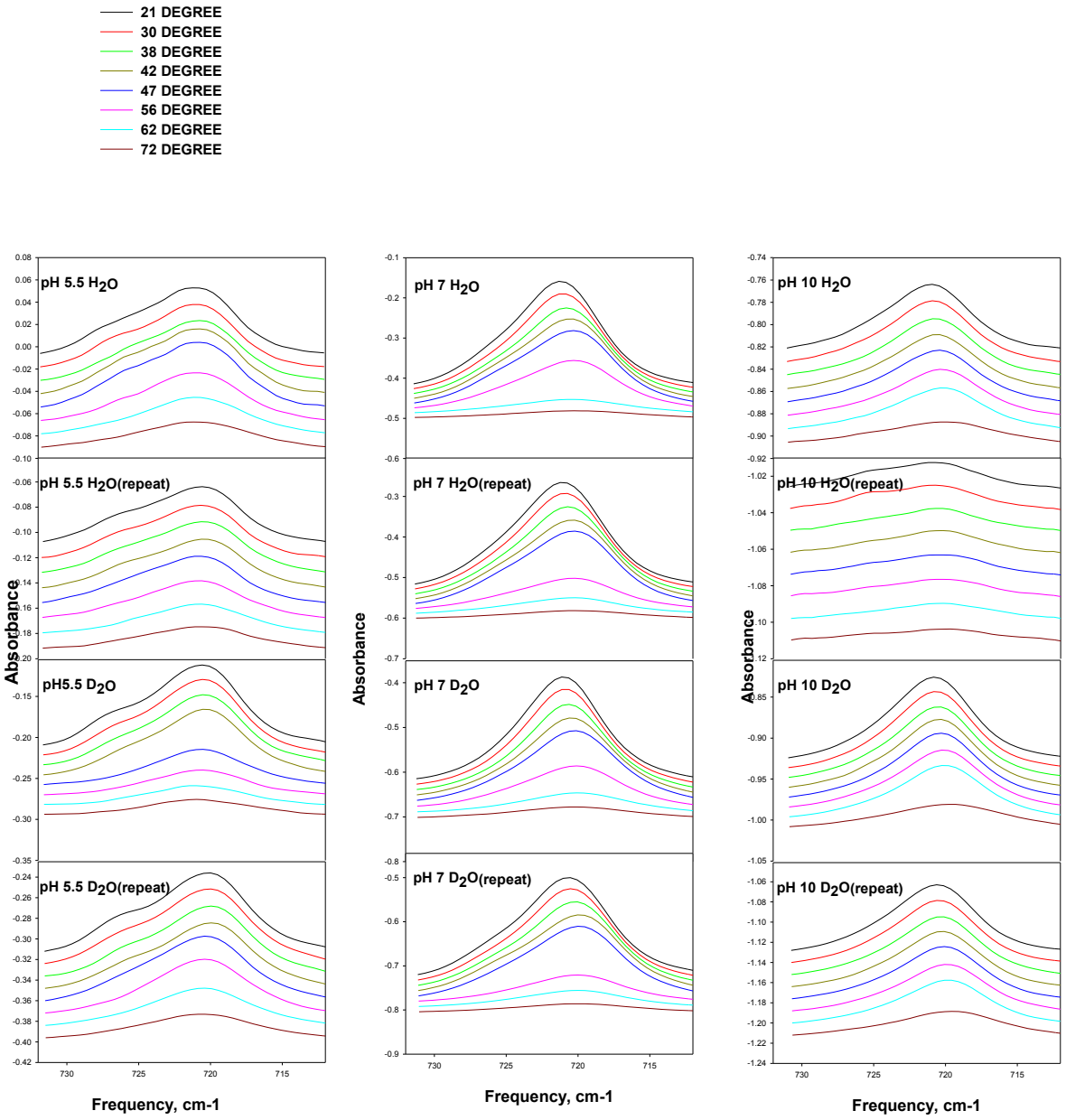

Figure 2.3 The original spectra of the ρCH_2 modes of equimolar mixtures of Cer/SA-d35/Chol measured as a function of temperature

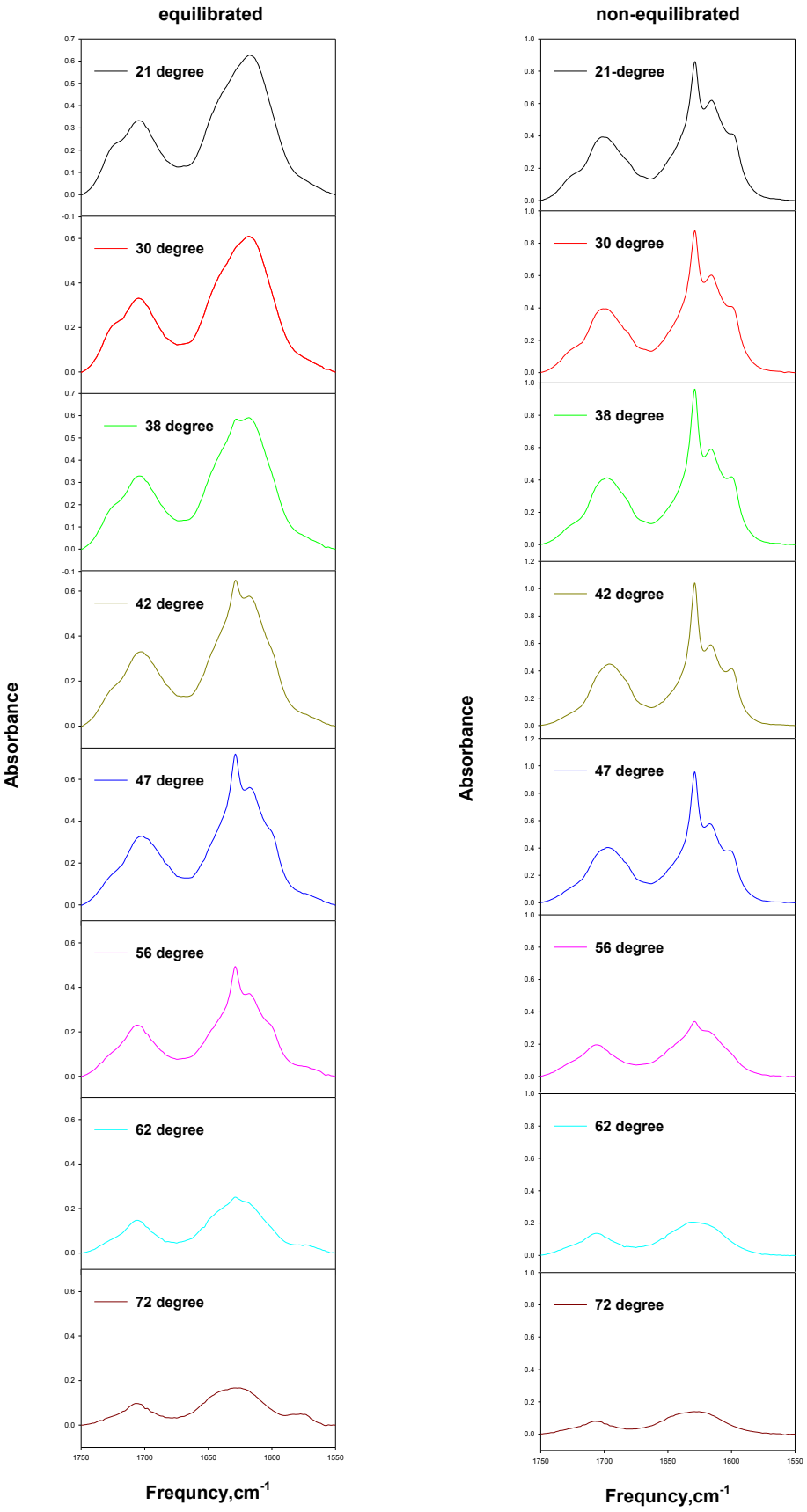

Figure 2.4 Two different kinetic behaviors of the Amide I vibrational region at pH7

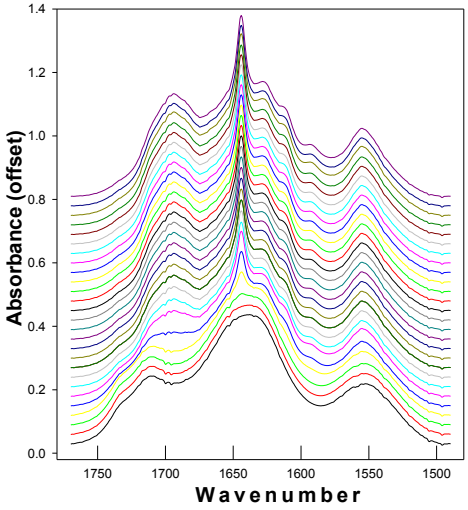
Absorbance (offset)
1.4
1.2
1.0
0.8
0.6
0.4
0.2
0.0
1750
1700
1650
1600
1550
1500
Wavenumber

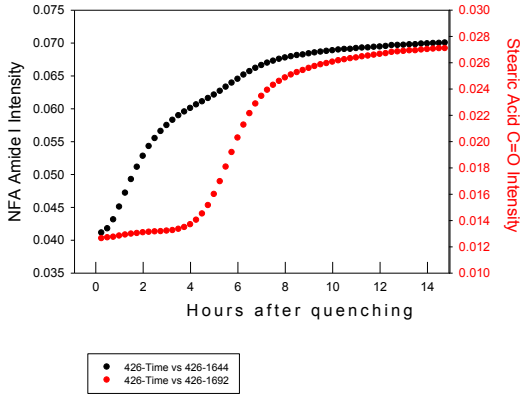
NFA Amide I Intensity
Stearic Acid C=O Intensity
Hours after quenching
426-Time vs 426-1644
426-Time vs 426-1692

(a)

(c)

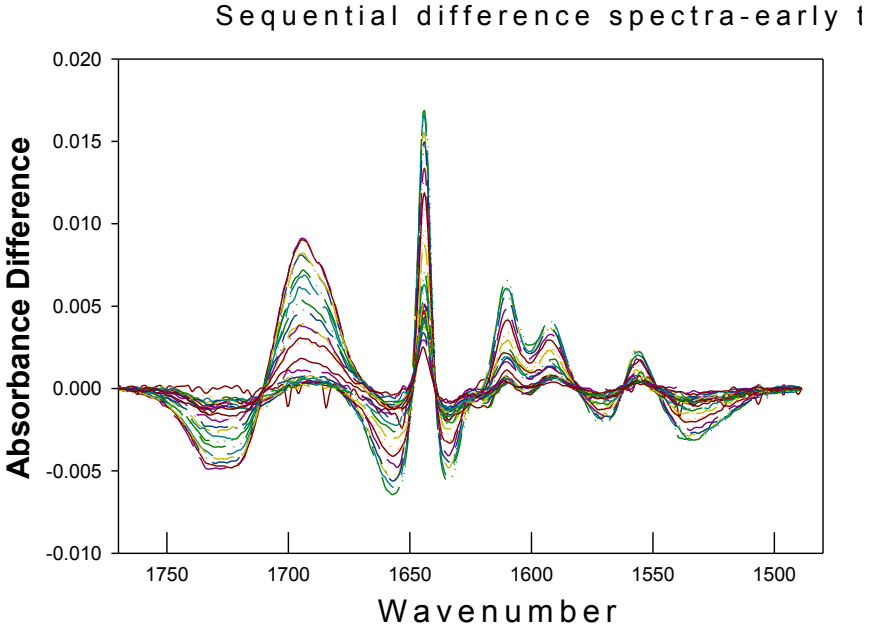
Sequential difference spectra-early t
Absorbance Difference
0.020
0.015
0.010
0.005
0.000
-0.005
-0.010
1750
1700
1650
1600
1550
1500
Wavenumber

(b)

Figure 2.5 (a) Time evolution of the Amide I region of ceramide and the carbonyl stretching region of fatty acid in the ternary model SC system quenched from 90°C to 31°C. (b) Time evolution of difference spectra constructed from the Amide I region and carbonyl stretching region data. The difference spectra were constructed by subtracting the first spectrum following quenching (lable"0") in part "a" from each spectrum following. (c) Time evolution of intensity in the Amide I (●left-hand scale) and in the carbonyl stretching (●right-hand scale)

indicating a transition from ordered to disordered phase at a T_m of 52°C and 56°C respectively at pH 5.5 and pH 7. In the case of Cer/SA-d_{35}/Chol at pH10, ν_sCH band is located above 2850 cm^{-1} between 20°C and 70°C and is followed by a sharp transition with T_m of 70°C. ν_s CH_2 band at pH10 is much higher than those at pH5.5 and pH7, which indicates the acyl chains are less ordered at pH10 at temperatures below Tm.

The methylene rocking modes provide information about the packing of the chains perpendicular to the chain direction. The short-range coupling between hydrocarbon chains in an orthorhombic lattice results in a splitting of the ρCH_2 or ρCD_2 vibration. The ρCH_2 vibration of the equimolar Cer/SA-d_{35}/Chol is plotted in Figure 2.3. At pH5.5, broadening of the contour at 20℃ is observed, which disappears at 47℃. The splitting is indicative of an ordered orthorhombic lattice. At pH7, Cer/SA-d_{35}/Chol mixtures reveals only a very slight broadening of ρCH_2 vibration in some cases. However at pH10, only one clear single peak is observed, suggesting that Cer/SA-d_{35}/Chol mixtures form a hexagonal lattice.

The two sets of data at pH7 show different kinetic behaviors. The region between 1540cm^{-1} and 1720cm^{-1} includes the Amide I vibrational mode of the ceramides at 1644cm^{-1} and the carbonyl stretching (COOH) of the fatty acid at 1692cm^{-1}. The

temperature dependence of Amide I vibration mode is plotted in Figure 2.4. One broad peak is observed in the left hand set before 38℃ indicating a disordered H-bonding, while a sharp peak arises from gradual splitting between 38℃ and 62℃, formation of an ordered strucuture. However, the sharp peak in the right hand set appears at all temperatures below 62℃. The result indicates that the equimolar ratio of Cer/SA-d_{35}/Chol at pH7 shows two different kinetic behaviors. To investigate the kinetics of the SC model, experiments were performed in which a SC model sample was warmed to 90℃ then quenched to 31℃. The time evolution of the line widths were monitored. Typical behavior of the time evolution of the Amide I vibrational mode is shown in part "a" of Figure 2.5. The reappearance of the 1644 cm^{-1} peak monitors the occurrence of ordered H-bonds in lipid phases. To aid in quantitative analysis of the time evolution of the 1644 cm^{-1} band, difference spectra are plotted in part "b" of Figure 2.5. These were calculated by subtracting the first spectrum following quenching from the spectrum at each succeeding time. The reappearance of the 1644 cm^{-1} feature becomes clearer when the data are plotted in this way. The time for domain formation in the ceramide was more rapid than in the fatty acid shown in parts "b" and "c" of Figure 2.5.

Part III IRRAS-Based Binding Assay for Lung Surfactant SP-D and Lipid Monolayers

3.1 Introduction

Pulmonary surfactant, a lipoprotein complex at the air/water (A/W) interface in the lung, plays an essential role in reducing surface tension; however, it is now also recognized as a critical component in lung immune host defense. Surfactant consists of over 90% lipids (with dipalmitoylphosphatidylcholine (DPPC) as the major lipid component) and 5-10% protein [with surfactant proteins (SP) A, B, C, D as major protein components]. Two of the major surfactant proteins, SP-A (28-36kDa) and SP-D (43kDa) [32], are members of a family of collagenous, calcium-dependent lectins (collectins). Both SP-A and SP-D bind a wide spectrum of pathogens including viruses, bacteria, fungi, and pneumocystis. In addition, both molecules have been measured in the systemic circulation by immunologic methods and may be useful biomarkers of disease.

Collectins are composed of four domains: 1) a cysteine-rich N-terminal noncollagenous domain, 2) a collagen-like domain, 3) an α-helical coiled-coil neck domain, and 4) a C-terminal (calcium dependent) carbohydrate recognition domain (CRD; lectin domain). Collectins are

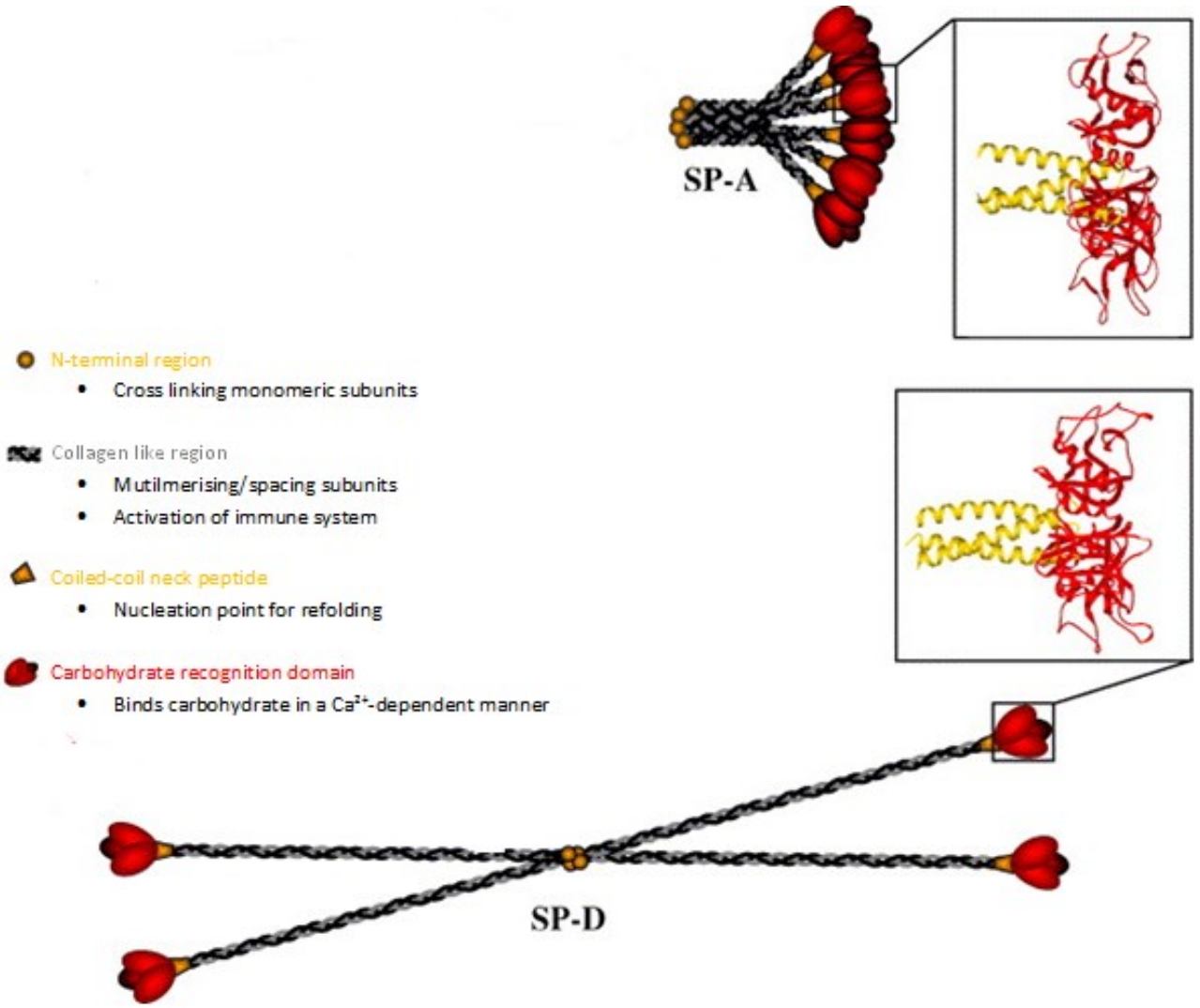

Figure 3.1 Protein structure of human SP-D and SP-A. Four domains are shown: the cysteine containing N-terminal region (orange), the collagen region (grey), the α-helical coiled-coil neck peptide (orange) and the CRD (red). [Kishore U et al. (2006) Surfactant proteins SP-A and SP-D structure, function and receptors *Molecular Immunology* 43(9): 1293-1315.]

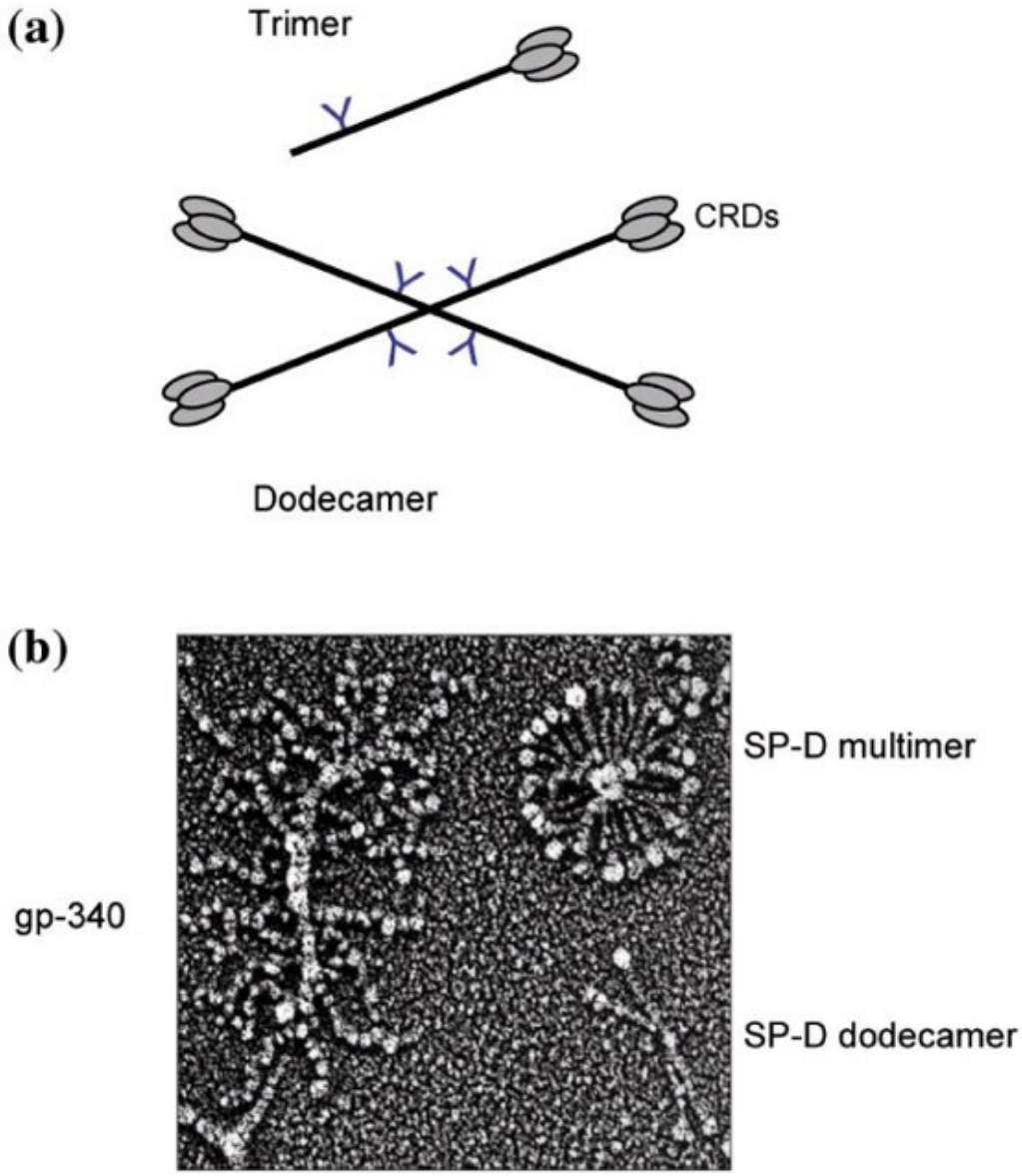

Figure 3.2 **(a)** Schematic diagram illustrating the structure of SP-D dodecamers, which consist of four trimeric subunits, and SP-D trimers. **(b)** Quick-freeze deep-etch image of human SP-D dodecamers, SP-D multimers, and the SP-D binding protein gp-340 (kindly provided by John Heuser, Washington University School of Medicine, St Louis, Missouri, USA).

trimetric polypeptide chains that are assembled into oligomers Figure 3.1.

SP-D assembles predominantly as dodecamers consisting of four trimetric subunits, although trimers and higher-order multimers have been observed Figure 3.2. SP-D binds to simple and complex saccharides, such as mannose, glucose or inositol, which are often found on the surface of microorganisms. Another binding target of SP-D is lipopolysaccharide (LPS), an essential component of Gram-negative bacterial outer membranes. LPS is composed of two parts: a well-conserved lipid A and a core oligosaccharide region that terminates in a less highly-conserved-O-polysaccharide chain. SP-D could interact with the glucose motif in a lipid A region and/or a core oligosaccharide region. SP-D can also interact with specific constituents of pulmonary surfactant containing phosphatidylinositol (PI) and glucosylceramide (GluCer). To investigate collectin-PI interaction, the following technical consideration must be overcome, namely the size and complexity of reactants and association products limit the applications of high resolution crystallography and NMR approaches.

Monolayers at the air/water (A/W) interface have become one of the best experimental paradigms for monitoring the interactions between the collectins and PI in the outer membrane of Gram-negative bacteria. At the A/W interface, the hydrophobic chains extend into the air, while the polar regions extend into the aqueous subphase as putative recognition sites for SP-D. From an experimental point of view, monolayer composition, surface pressure, molecular density, phase separation and domain formation can be easily controlled. Typically, an aqueous protein solution is injected into a Langmuir trough under a formed lipid monolayer followed by recording

surface pressure changes. This method provides some information about lipid/protein interaction.

IR and Raman spectroscopy are the best techniques to provide molecular level structure information from monolayers at the A/W interface. A technique termed infrared reflection-absorption spectroscopy (IRRAS), was developed specifically for examining aqueous monolayer films of lipids and proteins at A/W interface [33]. Along with IRRAS, standard Langmuir trough surface pressure measurements are made to valuate surface thermodynamics.

3.2 Experimental Methodology

Material

DOPI (ammonium salt), DPPI (ammonium salt), DPPC and Kdo2 (ammonium salt) were purchased from Avanti Polar Lipids,Inc. (Alabaster, Alabama). Chloroform, methanol, and HPLC-grade water were obtained from Fisher Scientist (Pittisburgh,PA). D_2O with 99% isotopic enrichment was purchased from Cambridge Isotope Laboratories (Andover,MA). The structures of all samples are shown in Figure 3.3.

A trimeric, recombinant human protein lacking heterologous N-terminal tags, SP-D NCRD (hNCRD), and a trimeric recombinant rat SP-D NCRD (rNCRD) fusion protein, were both provided by Prof. Erika Crouch (Washington University).

Sample preparations

DOPI was dissolved in chloroform/methanol (10/1,v/v) at ~0.5mg/mL concentration. DPPI was dissolved in chloroform at ~0.5mg/mL concentration. A Nima 611 LB trough (Nima Technology, Inc., Coventry, England, maximium surface area approximately 600 cm^2) with a model PS4 surface pressure sensor was used for the acquisition of monolayer surface pressure-molecular area (π-A) isotherms from the mixture of four components. Generally, 90ul of the DOPI solution or 120ul of the DPPI solution was spread on a 150 mM NaCl, 5 mM Tris (pH=7.1), and 4mM $CaCl_2$ subphase at 20°C at large molecular areas. Following a 30 min equilibration period to allow for solvent evaporation and film relaxation, monolayers were compressed at 15 cm^2/min while isotherms were recorded.

IRRAS measurement

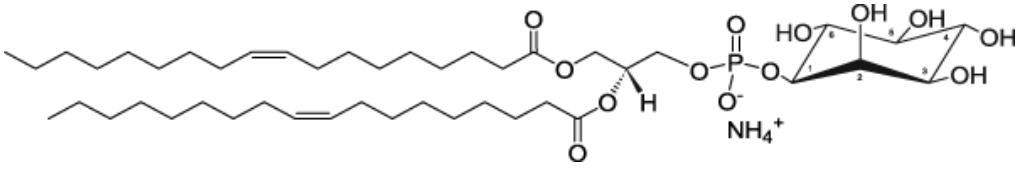

DOPI

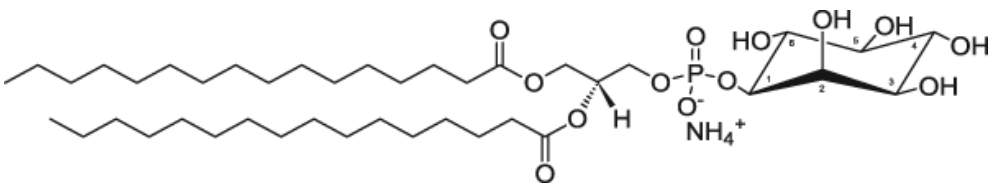

DPPI

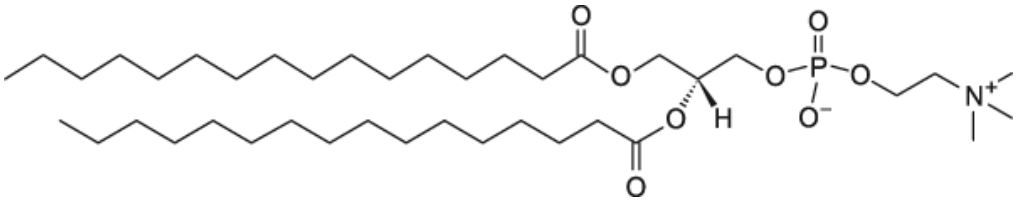

DPPC

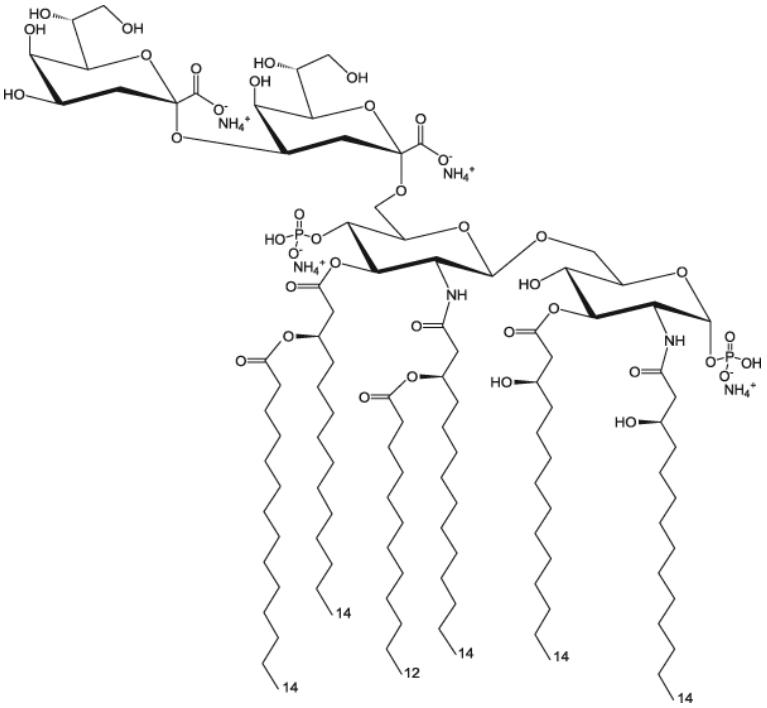

Kdo$_2$

Figure 3.3 The chemical structures of DOPI, DPPI, DPPC and Kdo$_2$

IRRAS spectra were acquired with a Bruker Instruments Equinox 55 spectrometer equipped with an external variable angle reflectance accessory, the XA511. The accessory is coupled to a custom-designed Langmuir trough (maximum area of 86 cm^2) constructed by Nima Technology Ltd. (Coventry,England) with a model PS4 surface pressure sensor. IRRAS spectra were acquired with a wire grid polarizer mounted in the optical path. Computer-driven stepper motors rotate the mirrors to obtain the desired angle of incidence. The reflected light is directed to a narrow band mercury/cadmium/telluride (MCT) detector. The whole experiment setup is enclosed and purged with nitrogen gas to keep the relative humidity low.

IRRAS spectra were collected with the use of a sample under computer control to compensate for the residual water vapor. For each spectrum, a total of 1024 scans were acquired at ~8 cm^{-1} resolution, in 2 blocks of 512 scans each, coadded, and apodized with a Blackman-Harris-3-term function, and fast Fourier transformed with one level of zero-filling to produce spectral data encoded at ~4 cm^{-1} intervals. IRRAS spectra were reported as $-\log(R/R_0)$, where R is the intensity of light reflected from the film-covered surface and R_0 is the intensity of light reflected from the background surface.

Experimental procedures are described as follows: Aliquots of 16 μL of DOPI (0.5mg/mL) solution were spread dropwise on D_2O-based subphase and 30 min were allowed for sample equilibration. The initial surface pressure for all experiments is 0 mN/m. Spectra were collected during intermittent compression while π-A isotherms were recorded at a barrier speed of 2 cm^2/min. The barrier was stopped at particular surface pressure values and a relaxation time of 5 min was allowed before collection.

For studies of SPD-NCRD adsorption, when the desired surface was reached (30mN/m), 50μL of the protein solution was injected beneath the preformed lipid monolayer. When the surface pressure stabilized (10~20 min), spectra of the lipid/protein films were acquired. Solutions of DOPI/DPPC-d_{62} (3/1, 22μL, 0.46mg/mL), DPPC (30μL, 0.4mg/mL), DPPI (25μL, 0.5mg/mL), KDo2 (30ul, 0.35mg/mL) and KDo_2/DPPC-d_{62} (1/1, 26μL, 0.36mg/mL) were examined with the same procedures.

Initially, Grams/32 software (Galactic Industries Corps, Salem, NJ USA) was utilized for baseline correction, smoothing, and determining peak intensity at particular frequencies with the amide I contour following baseline correction. RAMOP (supplied by NRC of Canada) is the other software which is used for picking the positions of the Amide I peak.

3.3 Results and Discussion

Initial IRRAS experiments were conducted to evaluate the sensitivity of spectra to protein binding. Phospholipid monolayers of varying composition and two recombinant trimeric NCRDs of SP-D were utilized for this purpose. In the first set of IRRAS experiments, lipids with specific headgroups were chosen where in-vitro CRD binding is known to occur with either high (PI) or low (PC) affinity [34]. In these experiments, the acyl chain composition of the phospholipids is the same. As described in the experimental section, lipid monolayers are compressed to a surface pressure of 30 mN/m before protein is injected into the subphase. This pressure is within the range

generally accepted for biological membranes and it is anticipated that lipid coverage of the air/water interface is essentially complete, preventing protein adsorption to the interface. The lack of a surface pressure increase upon protein injection supports this supposition. A lipid to protein (monomer) mole ratio of ~4:1 was used for all experiments unless otherwise noted. IRRAS spectra of the 1600-1780 cm^{-1} region encompassing the protein Amide I (~1650 cm^{-1}) and lipid carbonyl (~1735 cm^{-1}) modes are shown in Figure 3.4 for two different lipid monolayers, each with WT and NNK proteins. The Amide I vibration for the IRRAS experiments reported herein are represented as negative peaks in the spectra due to the optical set-up of the experiment (polarization of incident light and angle of incidence used) and the overall direction of the Amide I transition dipole moment change. Thus, when represented as the –log (R/Ro), IRRAS bands in the current set of experiments are negative. A wide range of variation in the Amide I intensity is evident in the figure and overall, is consistent with previous reports of binding assays [35] and lipid association in pulmonary surfactant (PS) [36]. Spectra for both WT and NNK injections under DPPI monolayers display Amide I intensity indicative of binding, albeit to different extents, whereas the lack of a significant Amide I band in the DPPC-d_{62} monolayer experiments after 1 hr indicates essentially no protein-lipid interaction. In addition, the contour of the lipid carbonyl band differs for the two lipid monolayers and for the most part is independent of the presence of protein. A nearly symmetric band at ~1735 cm^{-1} is observed for the DPPC monolayers indicating that the lipid carbonyl is in a relatively unhydrated state whereas

an additional low frequency component (~1720 cm^{-1}) indicative of a hydrated carbonyl is observed for the DPPI monolayers.

Figure 3.5 displays the integrated area of the Amide I band as a function of time after protein injection under various lipid monolayers initially compressed to a surface pressure of 30 mN/m. Areas are displayed as negative for negative-going peaks. In the Figure 3.6, a significant increase in Amide I intensity is observed for NNK compared to WT for the inositol-containing lipid monolayers while the differences for each protein binding to DPPI compared to DOPI are minor. The significantly larger

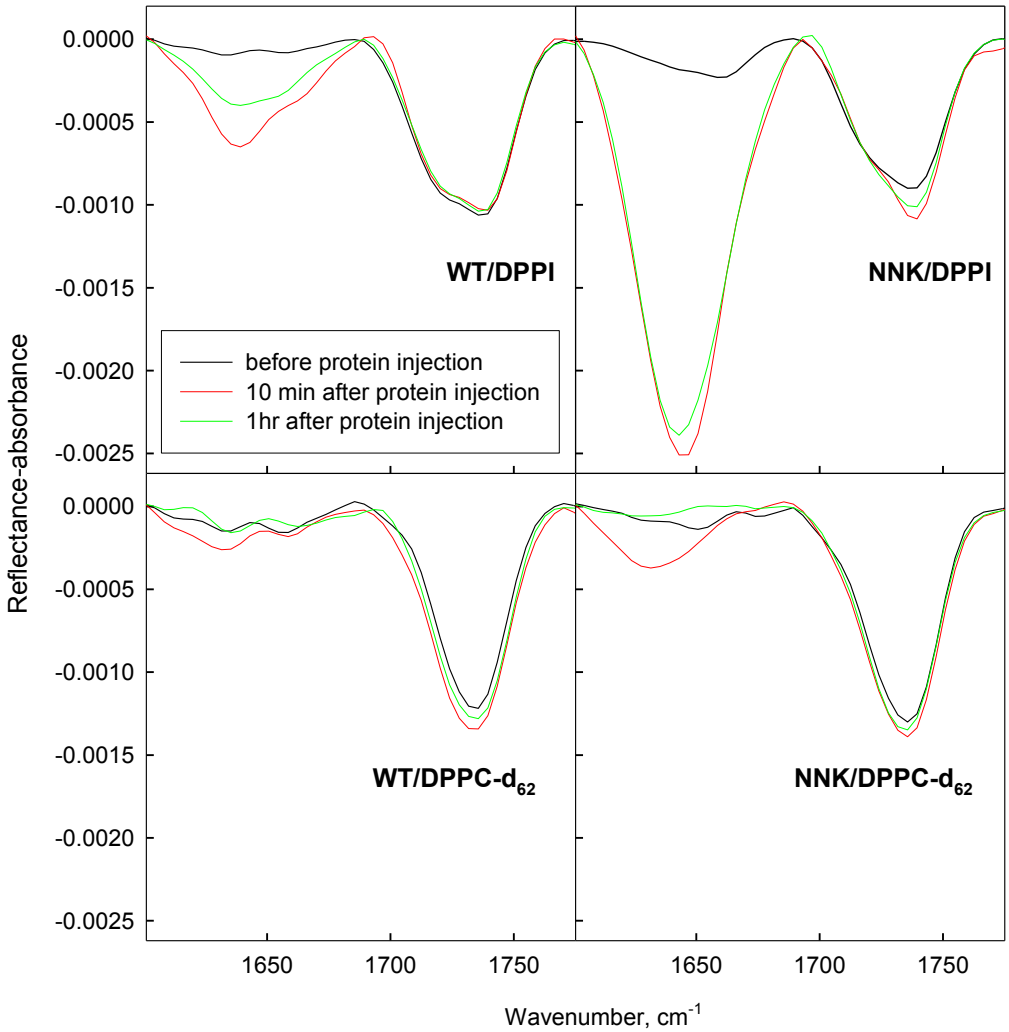

Figure 3.4: IRRAS spectra of protein amide I and lipid carbonyl region for DPPI and DPPC-d_{62} before and after NCRD (WT and NNK, as noted) injection into the subphase.

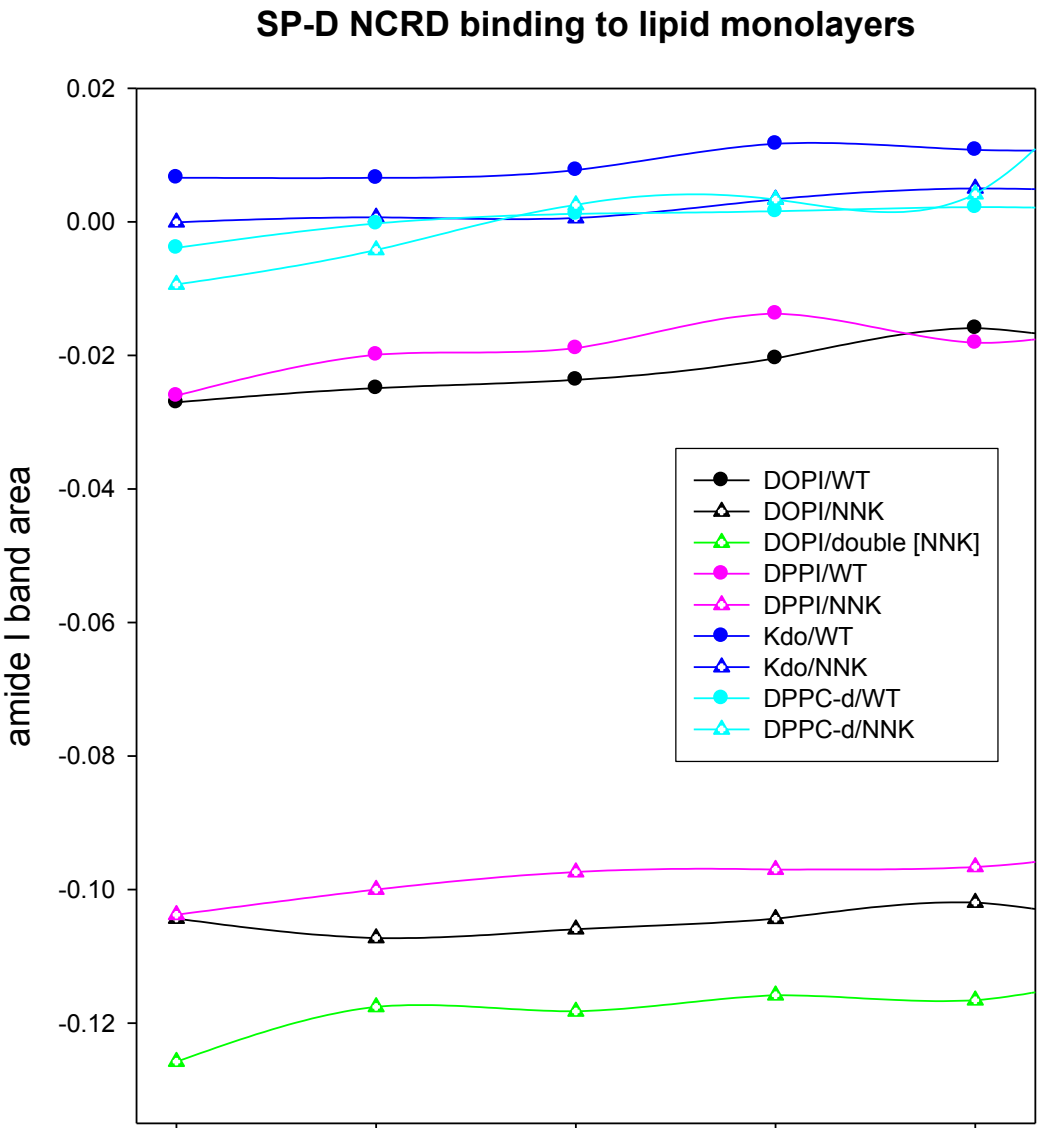

Figure 3.5: Amide I band area as a function of time after protein injection under lipid monolayers of varying composition.

Amide I area for NNK appears to reflect the species-dependent preference for myoinositol reported for homologous rat versus human trimeric NCRDs [35] [37], given that the NNK NCRD is modeled after rat SP-D. In contrast, very little Amide I intensity was observed for either protein when injected beneath DPPC-d_{62} or Kdo_2-lipid A monolayers. NNK dose-dependent DOPI binding was evaluated and the resulting Amide I band areas are also displayed in Figure 3.5. For a doubling of the NNK concentration, an increase of only ~13% (average area over first 40 min) was observed for the Amide I band area. The results indicate that the binding between DOPI and NNK is nearly saturated at the lower protein concentration. Overall, it appears as if IRRAS Amide I band areas can serve as a measure of ligand binding. The results are compatible with previous binding assays and lipid association in PS [34][37]. Indeed, the magnitude of the increase in the Amide I band area for NNK compared to WT (~5 fold) binding to either DOPI or DPPI is of the same order as that reported for rat versus human NCRD binding to maltose-substituted supports [37].

A few particular IRRAS experiments were conducted using isolated rat SP-D full length dodecamers (FL) for comparison with NCRDs. Although a lower molar concentration of monomers were used in the dodecamer experiments (lipid:protein monomer of 40:1), the Amide I band area was significantly higher than either WT or NNK NCRD binding experiments with a DOPI monolayer (see Figure 3.6). This may be due to both cooperative interactions between multiple trimers enhancing the binding of the dodecamers and also the close proximity of the collagen-like region of SP-D to the lipid monolayer enabling the IR beam to "sample" the full length protein molecule. The results shown in Figure 3.6 are the averages of the Amide I band area for spectra acquired over the first 40 minutes after protein injection. Consistent with previous binding assays, the Amide I band cannot be detected when a DPPC monolayer is present, providing strong evidence that non-specific protein adsorption does not occur in the current IRRAS experiments or does not lead to measurable Amide I intensities.

The potential influence that lipid acyl chain order and/or packing may have on protein binding can be evaluated by comparing Amide I band areas of each respective NCRD protein interacting with DPPI to DOPI. As previously noted, Figure 3.5 shows only minor differences in Amide I band areas when the results are observed the two PI monolayers are compared even though ordered packing of the acyl chains is severely disrupted for DOPI due to the presence of 9-cis C=C double bond in both chains. Evidence of this is observed in the steepness of the isotherms and by measuring the frequency of the methylene stretching modes. Figure 3.7 shows overlaid isotherms of

DOPI and DPPI. The steepness of the DPPI isotherm is indicative of a more condensed monolayer compared to the DOPI. In addition, the methylene asymmetric stretching

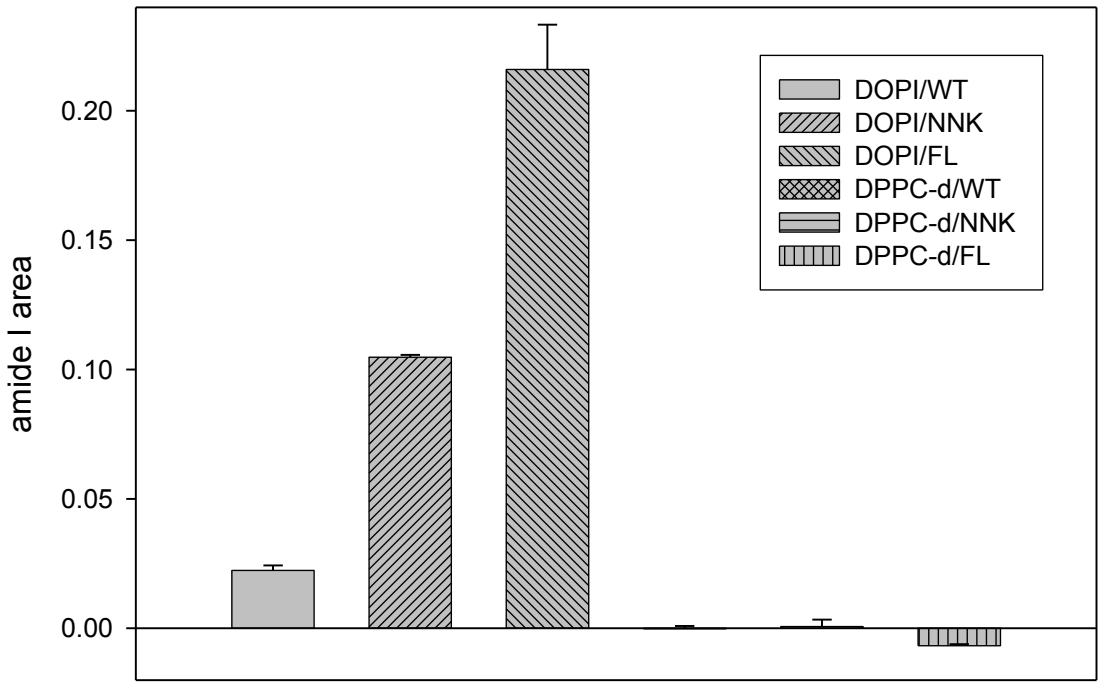

Figure 3.6: Average Amide I band area for spectra acquired over first 40 min. after protein injection into the subphase for lipid monolayers and proteins as noted.

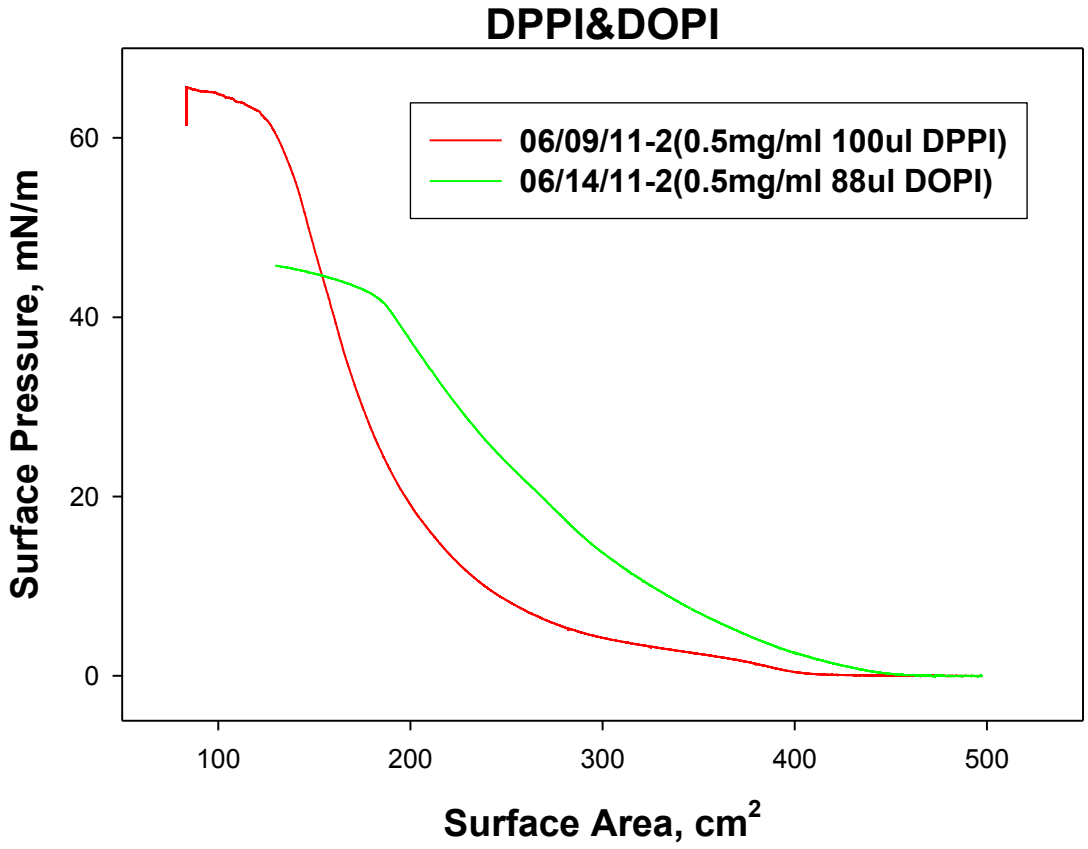

Figure 3.7: Surface pressure-area isotherms for DPPI and DOPI monolayers acquired under continuous compression. For IRRAS experiments, the barrier is stopped at

several surface pressure values (~ every 5 mN/m) while spectra are acquired. Protein is injected under the lipid monolayer at pressure of 30 mN/m.

frequency at surface pressure of 30 mN/m is ~2919 cm^{-1} for the DPPI monolayer compared with ~2925 cm^{-1} for DOPI, indicative of a significantly higher degree of acyl chain conformational order for the DPPI. Hence, ligand binding in the current set of experiments is essentially independent of lipid acyl chain order and/or packing.

IRRAS experiments to probe NCRD interaction with binary lipid monolayers imply that cooperativity among all three CRDs in a trimer is important for binding stability. Monolayers composed of approximately 3:1 (mol:mol) DOPI:DPPC-d_{62} were spread at the air/water interface and compressed to a surface pressure of 30 mN/m prior to protein injection. Perdeuteration of the acyl chains in DPPC allows spectroscopic detection of acyl chain conformational order for both lipid species via the CH_2 and CD_2 stretching band frequencies. Evidence of lipid mixing was observed as the CD_2 symmetric stretching frequencies were at least 4 cm^{-1} higher throughout compression for the mixed compared to single component monolayers (see Figure 3.8a). The magnitude of the frequency increase is indicative of a substantial decrease in DPPC-d_{62} acyl chain conformational order due to mixing with DOPI. Similarly, the methylene stretching frequencies of DOPI were observed to increase, albeit to a lesser extent, as the DPPC-d_{62} (minor component) imparts a slight ordering effect on the DOPI acyl chains in the mixed monolayers (not shown). Mixing of the lipids will decrease the density of inositol rings available for NCRD

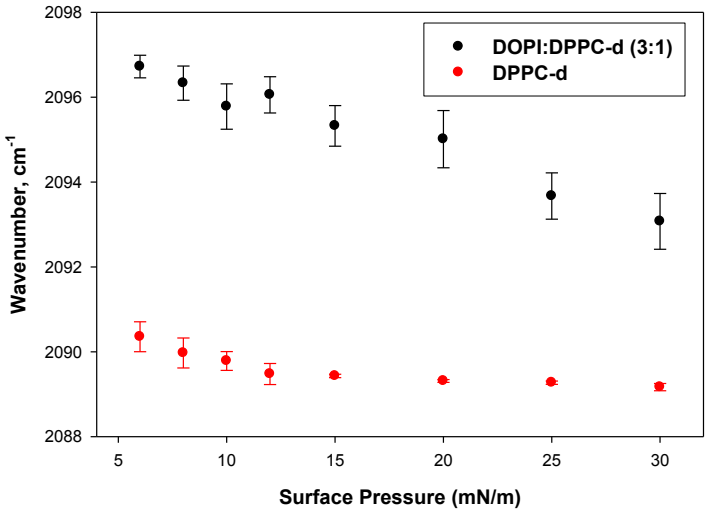

(a)

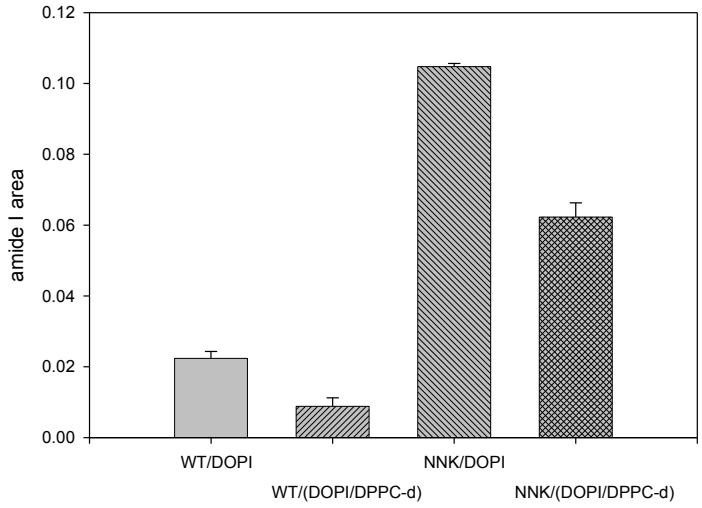

(b)

Figure 3.8: (a) Symmetric CD2 stretching band frequency as a function of surface pressure for a DPPC-d_{62} monolayer versus a 3:1 DOPI: DPPC-d_{62} monolayer. (b) Average Amide I band area for spectra acquired over first 40 min. after protein injection into the subphase for lipid monolayers and proteins as noted.

binding although for the ratio of lipids used, the number of inositol rings remains greater than the number of CRDs injected into the subphase. Figure 3.8b displays the average Amide I band area over the first 40 minutes after protein injection (for WT and NNK NCRDs) for pure DOPI versus the binary monolayers. For a 25% decrease in the amount of inositol present, a ~60% decrease in Amide I band area was observed for the WT NCRD and ~40% decrease for NNK NCRD. Hence, a decrease in inositol ring availability to a certain degree leads to a greater decrease in binding, suggesting that stability is provided by cooperative binding among CRDs.

References

[1] Proksch E, Brandner JM, Jensen JM. (2008).The skin: an indispensable barrier. *Exp. Dermatol*. 17(12): 1063–72.

[2] Madison KC. (2003). Barrier function of the skin: "la raison d'être" of the epidermis. *J. Invest. Dermatol.* 121(2): 231-41.

[3] Malvi *The Ageing Skin - Structure.*

[4] Marks JG, Miller J (2006). *Lookingbill and Marks' Principles of Dermatology* (4th ed.). 1–7.

[5] Fenske DB, Thewalt JL, Bloom M, Kitson N (1994). Models of stratum corneum intercellular membranes: 2H NMR of macroscopically oriented multilayers *Biophys. J.* 67(4): 1562–1573.

[6] Bouwstra JA, Honeywell-Nguyen PL, Gooris GS., Ponec M (2003) Structure of the skin barrier and its modulation by vesicular formulations *Progress in Lipid Research* 42: 1–36.

[7] Corvera E, Mouritsen OG, Singer MA, Zuckermann MJ (1992). The permeability and the effect of acyl chain length for phospholipid bilayers containing cholesterol. *Biochimica et Biophysica Acta*. 1107: 261-270.

[8] Bhattacharya S, Haldar S (2000). Interactions between cholesterol and lipids in bilayer membranes: Role of lipid headgroup and hydrocarbon chain-backbone linkage. *Biochimica et Biophysica Acta*. 1467: 39-53.

[9] Bouwstra JA, Gooris GS (2010). The Lipid Organisation in Human Stratum Corneum and Model Systems. *The Open Dermatology Journal,* 4: 10-13.

[10] Pilgram GSK, Engelsma-van Pelt AM, Oostergetel GT, Koerten HK, Bouwstra JA (1998). Study on the lipid organization of stratum corneum lipid models by (cryo-) electron diffraction. *The Journal of Lipid Research*,

39: 1669-1676.

[11] Caussin J, Gooris GS.; Bouwstra, JA (2008). BBA FTIR studies show lipophilic moisturizers to interact with stratum corneum lipids, rendering the more densely packed. *Biomembranes,* vol. 1778(6): 1517-1524.

[12] Damien F, Boncheva M (2010). The extent of the orthorhombic phase in stratum corneum determines the barrier efficiency of human skin *in vivo. J. Invest. Dermatol.* 130: 611-4.

[13] Barry BW (1988). Action of skin penetration enhancers—the Lipid Protein Partitioning theory. *International Journal of Cosmetic Science* 10(6): 281–293.

[14] Notman R, Noro M, O'Malley B, Anwar J (2004). Molecular simulation of the mechanism of action of oleic acid as a drug penetration enhancer. *Journal of Pharmacy and Pharmacology,* 56 (Suppl.1). S8-S9. ISSN 0022-3573.

[15] Ongpipattanakul B, Burnette RR, Potts RO, Francoeur ML (1991). Evidence that oleic acid exists in a separate phase within stratum corneum lipids. *Pharm Res.* 8(3): 350-4.

[16] Naik A, Pechtold L, Potts R, Guy R (1995). Mechanism of oleic acid-induced skin penetration enhancement in vivo in humans. *J Control Release*. 37(3): 299-306.

[17] Rowat AC, Kitson N, Thewalt JL (2006). Interactions of oleic acid and model stratum corneum membranes as seen by 2H NMR. *Int. J. Pharm.* 307(2): 225-31.

[18] Henry H, Mantsch DC *Infrared Spectroscopy of Biomolecules.*

[19] Mohammad AM (1999). Application of HPLC-FTIR Spectroscopy Using Thermospray Interface for Analysis of Anionic Surfactants. *Analytical Sciences* 15 (11): 1137-140.

[20] Moore DJ, Rerek ME, Mendelsohn R (1997). FTIR spectroscopy studies of the conformational order and phase behavior of ceramides. *The Journal of Physical Chemistry* B101: 8933.

[21] Snyder RG, Schachtchneider JH (1963). Vibrational analysis of the n-paraffins-I. Assignments of infrared bands in the spectra of C_3H_8 through n-$C_{19}H_{40}$. *Spectrochim. Acta*. 19: 85.

[22] Snyder RG, Strauss HL, Cates, DA (1995). Detection and measurements of microaggregation in binary mixtures of esters and of phospholipid dispersions. *J. Phys. Chem.* 99: 8432.

[23] Moore DJ, Rerek, ME, Mendelsohn R. (1997). Lipid domains and orthorhombic phases in model stratum corneum: evidence from fourier transform infrared

spectroscopy studies. *Biochemical and Biophysical Research Communications* 231: 797.

[24] Miyazawa T, Blout, ER (1961). Infrared spectra of polypeptides in various conformations: amide I and amide II bands. *J. Am. Chem. Soc.* 83: 712.

[25] Flach C, Mendelsohn R, Rerek ME, Moore DJ (2000). Biophysical studies of model stratum corneum lipid monolayers by infrared reflection-absorption spectroscopy and Brewster angle microscopy. *J. Phys. Chem. B*. 104(9): 2159-65.

[26] Gooris GS, Bouwstra JA (2007). Infrared Spectroscopic Study of Stratum Corneum Model Membranes Prepared from Human Ceramides, Cholesterol and Fatty Acids. *Biophysical Journal* 92: 2785-2795.

[27] Ananthapadmanabhan KP, Lips A, Vincent C, Meyer F, Caso C, Johnson A, Subramanyan K, Vetharmuthu M, Rattinger G, Moore DJ (2003). pH-induced alterations in stratum corneum properties. *Int. J. Cosm. Sci.* 25: 103-112.

[28] Schmid-Wendtner MH, Korting HC (2006). The pH of the skin surface and its impact on the barrier function. *Skin Pharmacol. Physiol*. 19: 296-302.

[29] Sparavigna A, Setaro M, Gualandri V (1999). Cutaneous pH in children affected by atopic dermatitis and in healthy children: a multicenter study. *Skin Res. Technol.* 5: 221-7.

[30] Bouwstra, JA, Gooris GS, Dubbellar FE, Weerheim AM, Ponec M (1998). pH,cholesterol sulfate, and fatty acids affect the stratum corneum lipid organization. *J. Inversting. Dermatol. Symp. Proc.* 3: 69-74.

[31] Potts RO, Francoeur ML (1993). *Drugs Pharm. Sci.* 59: 269.

[32] Pérez-Gil J, Keough KM (1998). Interfacial properties of surfactant proteins. *Biochim. Biophys. Acta.* 1408(2-3): 203–217.

[33] Flach CR, Brauner JW, Taylor JW, Baldwin RC, Mendelsohn R (1994): External reflection FTIR of peptide monolayer films in situ at the air/water interface: Experimental design, spectra-structure correlations, and effects of hydrogen-deuterium exchange. *Biophys.* 7(67): 402–41.

[34] Ikegami M, Grant S, Korfhagen T, Scheule RK, Whitsett JA (2009). Surfactant protein-D regulates the postnatal maturation of pulmonary surfactant lipid pool sizes. *J. Appl. Physiol.* 106: 1545–1552.

[35] Crouch E, McDonald B, Smith K, Roberts M, Mealy T, Seaton B, Head J (2007). Critical role of Arg/Lys343 in the species-dependent recognition of phosphatidylinositol by pulmonary surfactant protein D. *Biochemistry* 46: 5160–5169.

[36] Ogasawara Y, Kuroki Y, Akino T (1992). Pulmonary surfactant protein D specifically binds to phosphatidylinositol. *J. Biol. Chem.* 267(29): 21244–9.

[37] Crouch EC, Smith K, McDonald B, Briner D, Linders B, McDonald J, Holmskov U, Head J, Hartshorn K (2006). Species differences in the carbohydrate binding preferences of surfactant protein D. *Am. J. Respir. Cell Mol. Biol*. 35: 84–94.